XDH-1 inactivation causes xanthine stone formation in *C. elegans* which is inhibited by SULP-4-mediated anion exchange in the excretory cell

Jennifer Snoozy[1], Sushila Bhattacharya[1], Brandon Johnson[1], Robin R. Fettig[1,3], Ashley Van Asma[1], Chloe Brede[1], Sophia G. Miller[4], Martina Ralle[4], Kurt Warnhoff[1,2]

[1]Pediatrics and Rare Diseases Group, Sanford Research, Sioux Falls, SD 57104, USA

[2]Department of Pediatrics, Sanford School of Medicine, University of South Dakota, Sioux Falls, SD 57105 USA

[3]Department of Basic Biomedical Sciences, Sanford School of Medicine, University of South Dakota, Vermillion, SD 57069, USA

[4]Department of Molecular and Medical Genetics, Oregon Health & Science University, Portland, OR 97201, USA

Correspondence to: Kurt Warnhoff (kurt.warnhoff@sanfordhealth.org)

Abstract:

Xanthine dehydrogenase (XDH) is a molybdenum cofactor (Moco) requiring enzyme that catabolizes hypoxanthine into xanthine and xanthine into uric acid, the final steps in purine catabolism. Human patients with mutations in XDH develop xanthinuria which can lead to xanthine stones in the kidney, recurrent urinary tract infections, and renal failure. Currently there are no therapies for treating human XDH deficiency. Thus, understanding mechanisms that maintain purine homeostasis is an important goal of human health. Here, we used the nematode *C. elegans* to model human XDH deficiency using 2 clinically relevant paradigms: Moco deficiency or loss-of-function mutations in *xdh-1,* the *C. elegans* ortholog of XDH. Both Moco deficiency and *xdh-1* loss of function caused the formation of autofluorescent xanthine stones in *C. elegans*. Surprisingly, only 2% of *xdh-1* null mutant *C. elegans* developed a xanthine stone, suggesting additional pathways may regulate this process. To uncover such pathways, we performed a forward genetic screen for mutations that enhance the penetrance of xanthine stone formation in *xdh-1* null mutant *C. elegans*. We isolated multiple loss-of-function mutations in the gene *sulp-4* which encodes a sulfate permease homologous to human SLC26 anion exchange proteins. We demonstrated that SULP-4 acts cell-nonautonomously in the excretory cell to limit xanthine stone accumulation. Interestingly, *sulp-4* mutant phenotypes were suppressed by mutations in genes that encode for cystathionase (*cth-2)* or cysteine dioxygenase (*cdo-1*), members of the sulfur amino acid catabolism pathway required for production of sulfate, a substrate of SULP-4. We propose that sulfate accumulation caused by *sulp-4* loss of function promotes xanthine stone accumulation. We speculate that sulfate accumulation causes osmotic imbalance, creating conditions in the intestinal lumen that favor xanthine stone accumulation. Supporting this model, a mutation in *osm-8* that constitutively activates the osmotic stress response also promoted xanthine stone accumulation in an *xdh-1* mutant background.

Thus, our work establishes a *C. elegans* model for human XDH deficiency and identifies the sulfate permease *sulp-4* as a critical player controlling xanthine stone accumulation.

Background:

Purines are an abundant and fundamental metabolite class that are essential for the generation of RNA and DNA molecules and purine nucleotides are critical energy sources (ATP) and signaling molecules (GTP). Failures in purine metabolism can lead to both common and rare diseases. For instance, oncogenic mutations activate nucleotide biosynthetic capacity in diverse cancers, promoting cancer progression [1]. Mutations in enzymes in the purine metabolic pathway cause rare inborn errors of metabolism such as Lesch-Nyhan syndrome, purine nucleoside phosphorylase deficiency, and xanthinuria [2-5]. Thus, understanding the mechanisms that impact purine homeostasis is an important goal of human health.

Xanthinuria, an inborn error of purine metabolism, is caused by inactivation of xanthine dehydrogenase (XDH), the terminal enzyme in purine catabolism that oxidizes hypoxanthine to xanthine and xanthine to uric acid [6] (**Fig. 1A**). There are two types of human xanthinuria; type I is caused by mutations in the gene encoding the xanthine dehydrogenase enzyme and type II is caused by mutations in genes essential for the synthesis of the molybdenum cofactor, an essential prosthetic group for XDH [4, 5]. Both forms of xanthinuria present with high levels of xanthine in the urine and low levels of uric acid which can result in the formation of xanthine stones in kidneys and muscles, sometimes causing renal failure. There is currently no curative therapy for xanthinuria, however high fluid intake and low purine diets are recommended for patients [7].

Molybdenum cofactor (Moco) is an essential prosthetic group required for development in animals ranging from the nematode *C. elegans* to humans [4, 8]. Moco is synthesized by an ancient and conserved biosynthetic pathway [9]. *C. elegans* has recently emerged as a powerful model system for studying Moco biology, and the genes that encode the Moco biosynthetic enzymes are termed *moc* in *C. elegans* for MOlybdenum Cofactor biosynthesis [8, 10]. In addition to endogenous Moco synthesis, *C. elegans* can also acquire and use Moco from its bacterial diet [8, 11, 12]. Given its genetic tractability and the ability to manipulate animal Moco content by simple dietary manipulation, *C. elegans* is a useful model for understanding the biology of Moco and Moco-requiring enzymes, such as XDH-1 (**Fig. 1A**).

Here, we genetically explored the formation of xanthine stones in *C. elegans,* which emerged during Moco deficiency or in *xdh-1* mutant *C. elegans,* mirroring type I and type II human xanthinuria [4, 5]. Surprisingly, only a small percentage of Moco-deficient and *xdh-1* mutant *C. elegans* developed xanthine stones, suggesting additional parallel pathways for limiting stone formation. To identify novel regulators of xanthine stone accumulation, we performed an unbiased chemical mutagenesis screen for mutations that enhanced the penetrance of xanthine stone formation in *xdh-1* mutant animals. In this screen we recovered five loss-of-function alleles of *sulp-4,* a gene which encodes a member of the sulfate permease family of transporters with homology to human SLC26 transporters [13]. We demonstrated that SULP-4 acts in the *C. elegans* excretory cell, analogous to the human kidney, to inhibit the accumulation of

xanthine stones [14]. We further showed that *sulp-4* was required for normal development. Interestingly, we found that phenotypes caused by *sulp-4* loss of function were suppressed by inactivating mutations in *cth-2* or *cdo-1,* genes that encode core members of the sulfur amino acid catabolism pathway (**Fig. 1A**) [8]. We suggest that *sulp-4* loss of function causes sulfate accumulation. Disruption of *cth-2* or *cdo-1* impairs endogenous sulfate production, thereby suppressing the phenotypes observed in *sulp-4* mutant animals. Sulfate accumulation may cause an osmotic imbalance that leads to an increased rate of xanthine stone formation in the intestinal lumen. This model is supported by our observation that a mutation in *osm-8*, a key regulator of osmotic homeostasis, also promoted xanthine stone accumulation in an *xdh-1* mutant background [15]. Thus, our work establishes a *C. elegans* model for the rare genetic disease xanthinuria and identifies *sulp-4* as a potent genetic modifier of this disease pathology in *C. elegans,* likely acting through disrupted osmotic homeostasis.

Results:

XDH-1 inactivation caused the accumulation of xanthine stones in *C. elegans*.

To explore the pathology of Moco deficiency in the nematode *C. elegans,* we cultured *cth-2; moc-1* and *moc-1 cdo-1* double mutant animals on wild type (Moco replete) or *ΔmoaA* mutant (Moco deficient) *E. coli*. The *moc-1* mutation prevents the endogenous synthesis of Moco while the *cth-2* and *cdo-1* mutations suppress the lethality typically associated with animal Moco deficiency [8]. *cth-2* encodes cystathionase which converts cystathionine to cysteine and *cdo-1* encodes cysteine dioxygenase which oxidizes cysteine to cysteinesulfinate ultimately producing sulfites (**Fig. 1A**). Sulfites are extremely reactive and are detoxified to sulfate by the Moco-requiring sulfite oxidase (SUOX-1) enzyme. Thus, by changing the dietary *E. coli*, we can control whether the animals have Moco. When culturing *cth-2; moc-1* double mutant animals on Moco- *E. coli* we surprisingly observed animals that developed autofluorescent stones, typically found in the posterior of the intestine. 54% of *cth-2; moc-1* animals fed a Moco- diet developed an autofluorescent stone while 0% of *cth-2; moc-1* animals developed an autofluorescent stone when fed a diet that provided Moco. We observed similar results for *moc-1 cdo-1* double mutant animals where 17% of animals developed an autofluorescent stone on Moco- *E. coli* and 0% developed a stone when fed wild-type *E. coli* (**Fig. 1B**). Thus, we conclude that the formation of these autofluorescent stones is caused by Moco deficiency.

Surprisingly, we also observed the formation of autofluorescent stones in 8% of wild-type *C. elegans* when cultured on Moco- *E. coli.* 0% of wild-type animals developed an autofluorescent stone when fed Moco+ *E. coli* (**Fig. 1B**). This result demonstrates that dietary Moco deficiency alone is sufficient to promote the formation of autofluorescent stones. This result is surprising as wild-type animals are still competent to produce Moco through their endogenous biosynthetic pathway. However, these data are consistent with our recent findings that the *C. elegans* diet plays a significant role in promoting Moco homeostasis [12].

110 Given that the development of these autofluorescent stones was dependent upon dietary Moco
111 deficiency, we reasoned that the phenotype was likely being caused by inactivation of one of the four
112 animal Moco-requiring enzymes (sulfite oxidase, xanthine dehydrogenase, aldehyde oxidase, and
113 mitochondrial amidoxime reducing component) [9]. Interestingly, inactivation of the Moco-requiring enzyme
114 xanthine dehydrogenase causes the accumulation of insoluble and fluorescent xanthine stones in
115 organisms as diverse as plants, fruit flies, and humans [5, 16-20]. We therefore hypothesized that the
116 autofluorescent stones we observed during *C. elegans* Moco deficiency were xanthine stones. To test this,
117 we looked for the presence of autofluorescent stones in animals carrying the *ok3234* null mutation in *xdh-*
118 *1,* the *C. elegans* orthologue of xanthine dehydrogenase*.* In *C. elegans,* XDH-1 is expressed in the
119 intestine, excretory cell, and neurons [21]*.* When we cultured *xdh-1* null mutant *C. elegans* on wild-type *E.*
120 *coli* we indeed observed the formation of highly autofluorescent stones in 2% of animals (**Fig. 1B,C**). Thus,
121 *xdh-1* was necessary for inhibiting the formation of autofluorescent stones. Consistent with their presence
122 in diverse models of XDH-1-deficiency, we propose that the autofluorescent stones we observe during
123 Moco- and XDH-1- deficiency in *C. elegans* are xanthine stones.

124 ***sulp-4* inhibited the formation of xanthine stones.**

125 XDH-1 functions at the end of the purine catabolism pathway to oxidize hypoxanthine to xanthine
126 and xanthine to uric acid (**Fig. 1A**). Given the critical position of XDH-1 in purine metabolism, we were
127 surprised that only 2% of *xdh-1* null mutant animals developed a xanthine stone. This result suggests the
128 existence of parallel pathways for maintaining purine homeostasis. To identify additional regulators of
129 purine metabolism, we performed an unbiased chemical mutagenesis screen for mutations that enhanced
130 the penetrance of the xanthine stone phenotype. We mutagenized *xdh-1* mutant *C. elegans* with ethyl
131 methanesulfonate (EMS) and cultured the newly mutagenized animals for 2 generations allowing newly
132 induced mutations to become homozygous [22]. We then cloned single mutagenized F2 animals onto their
133 own petri dish and screened for clones where we observed a high fraction of F3 progeny developing
134 xanthine stones.

135 Here we describe five new EMS-induced recessive loss-of-function mutations that caused a high
136 penetrance of xanthine stone formation in an *xdh-1* mutant background, *rae299, rae302, rae319, rae320*
137 and *rae326* (**see Methods**). These mutant alleles were prioritized because they displayed strong
138 enhancement of xanthine stone formation and formed a complementation group, indicating they affect a
139 single gene (**see Methods**). To identify the causative genetic lesion in these new mutant strains, genomic
140 DNA from all five strains was analyzed via whole genome sequencing. Our complementation studies
141 suggested that the mutant strains should have novel mutations in a common gene. Only one gene, *sulp-4,*
142 was uniquely mutated in all five strains, strongly suggesting these mutations were causative for the
143 enhanced penetrance of xanthine stone formation in the *xdh-1* mutant animals (**Fig. 2A,B, Table S1**).
144 Among the newly isolated *sulp-4* alleles we found 3 missense and 2 splice site mutations. Based on their
145 recessive nature and molecular identities, we propose that these are loss-of-function alleles of *sulp-4.*

146 To test the hypothesis that loss of *sulp-4* function causes enhanced xanthine stone accumulation in
147 an *xdh-1* mutant, we used CRISPR/Cas9 to engineer a new *sulp-4* deletion allele, *rae334* [23, 24]. The
148 *sulp-4(rae334)* allele is a 683 bp deletion that eliminates part of exon 1, all of exons 2 and 3, and part of
149 exon 4 (**Fig. 2A**). Thus, we propose that *sulp-4(rae334)* encodes a null allele. The *sulp-4(rae334)* allele
150 strongly enhanced the penetrance of xanthine stone formation in *xdh-1* mutant *C. elegans,* phenocopying
151 the *sulp-4* alleles isolated in our EMS screen (**Fig. 2B**). These data demonstrate that the *sulp-4* lesions
152 identified by whole genome sequencing cause xanthine stone accumulation in *xdh-1* mutant animals.
153 Furthermore, these data show that *sulp-4* acts in parallel with *xdh-1* to inhibit the accumulation of xanthine
154 stones.
155 The xanthine stones observed in *xdh-1; sulp-4* double mutant animals localized to the posterior of
156 the *C. elegans* intestinal lumen, consistent with the localization of the stones observed in *xdh-1* mutant
157 animals (**Fig. 2C**)**.** In addition to observing xanthine stones at a higher frequency in *xdh-1; sulp-4* mutant
158 animals, the xanthine stones were also much larger suggesting that *sulp-4* loss of function enhances both
159 the penetrance and expressivity of the xanthine stone phenotype in *xdh-1* mutant animals (**Fig. S1**). This
160 may reflect an increased quantity of xanthine in stones displayed by *xdh-1; sulp-4* mutant animals when
161 compared to *xdh-1* single mutant animals.
162 We originally observed the formation of xanthine stones during conditions of Moco deficiency; *cth-*
163 *2; moc-1* double mutant animals feeding on Moco- *E. coli.* We hypothesized that the *sulp-4* mutation would
164 also enhance the formation of xanthine stones caused by Moco deficiency. To test this, we assayed
165 xanthine stone formation in *sulp-4* single mutant animals cultured on wild-type or Moco- *E. coli*. 89% of
166 *sulp-4* mutant animals developed xanthine stones during dietary Moco deficiency compared to 1% of *sulp-*
167 *4* mutant animals fed a Moco replete diet (**Fig. S2A**). These data are consistent with our conclusion that
168 *sulp-4* functions to limit the accumulation of xanthine stones caused by XDH-1 inactivation resulting from
169 either Moco insufficiency or an *xdh-1* mutation.
170 ***sulp-4* promoted healthy larval and embryonic development.**
171 While culturing the *sulp-4(rae334)* mutant strain, we observed that mutant animals were sick and
172 slow growing. Thus, we explored the role of *sulp-4* in development and embryonic viability. To test the
173 impact of *sulp-4* loss of function on developmental rate, we synchronized wild-type, *sulp-4(rae319),* and
174 *sulp-4(rae334)* animals at the first stage of larval development and assayed their growth after 72 hours.
175 We found that *sulp-4(rae334)* animals displayed a severe developmental delay compared to the wild type
176 (**Fig. 2D**). After 72 hours growth from L1, 100% of wild type animals reached the young adult stage (*n*=21),
177 Only 5% of *sulp-4(rae334)* animals reached the young adult stage with 47.5% reaching L4 and the
178 remaining 47.5% failing to reach L4 (*n*=24). Interestingly, *sulp-4(rae319)* animals showed a more subtle
179 developmental delay (38% young adult, 58% L4, 4% pre-L4, *n*=21, **Fig. 2D**). Thus, we propose that *sulp-*
180 *4(rae334)* is a null allele while *sulp-4(rae319)* represents a hypomorph. Similarly, we observed that *sulp-*
181 *4(rae334)* caused 18% embryonic lethality while *sulp-4(rae319)* caused 5% embryonic lethality. No
182 embryonic lethality was observed for wild-type *C. elegans* (**Fig. 2E**). Thus, we conclude that *rae334* and

183 *rae319* represent an allelic series for *sulp-4* and that *sulp-4* is necessary for promoting embryonic and
184 larval development in *C. elegans.*

185 ***pnp-1* was necessary for the formation of xanthine stones in *xdh-1; sulp-4* mutants animals.**

186 To further test the model that the autofluorescent stones observed in *xdh-1; sulp-4* mutant animals
187 were composed of xanthine, we performed genetic epistasis with a null mutation in purine nucleoside
188 phosphorylase (*pnp-1*), a gene necessary for the formation of hypoxanthine and xanthine (**Fig. 1A**) [25].
189 PNP-1 is expressed and acts in the *C. elegans* intestine in addition to expression in some head neurons
190 [25]. As previously observed, *xdh-1; sulp-4* double mutant animals displayed 98% autofluorescent stone
191 formation while *pnp-1 xdh-1; sulp-4* triple mutant *C. elegans* displayed 3% formation of autofluorescent
192 stones (**Fig. 3A**). Thus, *pnp-1* was necessary for the formation of the autofluorescent stones observed in
193 *xdh-1; sulp-4* double mutant animals. Given that *pnp-1* plays a conserved role in the formation of
194 hypoxanthine and xanthine, these results support our model that the autofluorescent stones we observe
195 are likely to be predominantly composed of xanthine. Although, we cannot exclude the possibility that
196 other metabolites, such as hypoxanthine, are also present in the autofluorescent stones.

197 To determine if *pnp-1* acts in a genetic pathway with *sulp-4,* we tested the impact of *pnp-1* loss of
198 function on the developmental delay displayed by *sulp-4* mutant animals. *pnp-1; sulp-4* double mutant
199 larvae developed at a rate similar to *sulp-4* single mutant animals (**Fig 3B**). After 72 hours growth from L1,
200 81% of *pnp-1; sulp-4* double mutant animals reached the young adult stage while the remaining 19%
201 reached L4 (*n*=31). Similarly, 83% of *sulp-4* single mutant animals reached young adult, 14.5% reached L4
202 and 2.5% failed to reach L4 (*n*=42). Importantly, *pnp-1* mutant animals displayed healthy larval
203 development (100% young adults 72 hours post L1, n=39, **Fig. 3B**). Thus, *pnp-1* was not required for the
204 developmental delay displayed by *sulp-4* mutant *C. elegans.* We propose a genetic pathway where *pnp-1*
205 promotes the formation of xanthine stones epistatic to the function of *xdh-1* and in parallel to the activity of
206 *sulp-4*.

207 ***sulp*-4/SLC26 encodes a sulfate permease that acted in the excretory cell to promote xanthine**
208 **homeostasis.**

209 *sulp-4* encodes a transmembrane transporter with homology to the SLC26 family of anion
210 transporters in mammals [13, 26]. The *C. elegans* genome encodes eight members of the SLC26
211 transporter family, named SULP-1 through SULP-8 [13]. We wondered if other members of the SLC26
212 family of transporters also played a role in limiting the formation of xanthine stones. To test this, we
213 cultured strains with deletions in *sulp-1, sulp-2, sulp-4, sulp-5, sulp-7,* and *sulp-8* on Moco- *E. coli* and
214 assayed the formation of xanthine stones. *sulp-3* and *sulp-6* mutant strains were not analyzed as they are
215 inviable. Only the strain carrying the *sulp-4* mutation displayed a high penetrance of xanthine stones (88%,
216 **Fig. S2B**). Thus, the enhancement of xanthine stone formation is specific to loss of *sulp-4* and not a
217 general feature of *sulp* inactivation.

218 SULP-4 is expressed in the apical membrane of the *C. elegans* excretory cell, a single cell that
219 plays roles in ionic regulation and waste elimination analogous to the mammalian renal system [13, 14,

220 27]. Studies of SULP-4 expressed in *Xenopus* oocytes demonstrate that SULP-4 is sufficient to promote
221 the transport of sulfate and, to a lesser extent, chloride [13]. To determine the site of action of *sulp-4* with
222 respect to the xanthine stone formation phenotype, we generated transgenic *xdh-1; sulp-4* double mutant
223 *C. elegans* expressing a *Psulp-4::SULP-4::GFP* translational fusion transgene (plasmid was a gift from Dr.
224 Keith Nerhke) [13]. Consistent with previous reports, we exclusively saw expression of the *Psulp-4::SULP-*
225 *4::GFP* translational fusion in the excretory cell (**Fig. 4A,B**). To test the functionality of the *Psulp-4::SULP-*
226 *4::GFP* transgene, we performed rescue experiments with *xdh-1; sulp-4* double mutant animals expressing
227 *Psulp-4::SULP-4::GFP* and assaying the formation of xanthine stones. *xdh-1; sulp-4* double mutant
228 animals expressing *Psulp-4::SULP-4::GFP* did not develop xanthine stones, demonstrating functional
229 transgenic rescue. This rescue was observed in three independently derived transgenic strains (**Fig. 4C**).
230 Thus, the *Psulp-4::SULP-4::GFP* transgenic fusion protein was functional, suggesting that its expression
231 pattern faithfully represents endogenous SULP-4 localization. We conclude that SULP-4 acts in the
232 excretory cell to negatively regulate the formation of xanthine stones. Our observation that *xdh-1; sulp-4*
233 double mutant animals develop xanthine stones in the intestinal lumen suggests that *sulp-4* is functioning
234 cell non-autonomously to limit the formation of xanthine stones.
235 To further test the role of the excretory cell in preventing the formation of xanthine stones, we used
236 an *exc-5* mutation that causes defects in excretory cell development and morphology [28]. We reasoned a
237 malformed excretory cell may not function efficiently and thus phenocopy *sulp-4* loss of function with
238 respect to xanthine stone formation. Indeed, *exc-5; xdh-1* double mutant animals displayed enhanced
239 formation of xanthine stones (**Fig. S3A**)**.** Although, the xanthine stone penetrance of the *exc-5; xdh-1*
240 (17%) double mutant strain was modest compared to *xdh-1; sulp-4*. Importantly, *sulp-4* loss of function did
241 not cause cysts in the excretory cell tubules, a severe defect in excretory cell morphology caused by *exc-5*
242 loss of function (**Fig. S3B-D**)**.** Although, we cannot exclude a subtle defect in excretory cell tubule
243 extension in *sulp-4* mutant animals. We conclude that the enhancement of xanthine stone formation
244 caused by inactivating mutations in *sulp-4* result from loss of SULP-4 anion exchange function and not
245 broader defects in excretory cell biology.
246 Furthermore, ion homeostasis plays a key role in the defecation cycle which promotes waste
247 elimination from the *C. elegans* intestine [29]. We wondered if the enhanced formation of xanthine stones
248 observed in *xdh-1; sulp-4* animals might result from failures in defecation, leading to xanthine
249 accumulation in the intestinal lumen and xanthine stone formation. To test this model, we used the *aex-*
250 *5(sa23)* mutation which causes defects in anterior body-wall muscle contraction (aBoc) and waste
251 expulsion (Exp), critical aspects of the defecation cycle [30]. Interestingly, *aex-5; xdh-1* double mutant
252 animals did not display an increased penetrance of xanthine stone formation (**Fig. S3A**). These results
253 suggest that defects in defecation alone are not sufficient to promote xanthine stone accumulation.
254 ***cth-2* and *cdo-1* were necessary for *sulp-4* mutant phenotypes*.***
255 *sulp-4* inactivation caused xanthine stone formation during dietary Moco deficiency (**Fig. S2A, Fig.**
256 **S4**), demonstrating that the enhancement of xanthine stones caused by *sulp-4* loss of function occurs

257 even when endogenous Moco biosynthesis is functional. To test the impact of a *sulp-4* mutation on
258 xanthine stone formation during complete Moco deficiency, we engineered *sulp-4; cdo-1 moc-1* triple
259 mutant *C. elegans* that cannot synthesize their own Moco (caused by *moc-1* mutation) and are viable
260 during Moco deficiency (caused by *cdo-1* suppressor mutation) (**Fig. 1A**). When cultured on Moco- *E. coli,*
261 *sulp-4; cdo-1 moc-1* triple mutants are completely Moco deficient yet only displayed 9% penetrance of
262 xanthine stones (**Fig. S4**). Similarly, *sulp-4; cdo-1* double mutant animals cultured on Moco- *E. coli*
263 displayed 0% penetrance of xanthine stones, dramatically reduced compared to the 86% penetrance
264 displayed by *sulp-4* mutant animals cultured on Moco- *E. coli* (**Fig. S4**). These results were surprising and
265 suggest that *cdo-1* is necessary for the formation of xanthine stones caused by a *sulp-4* mutation and
266 Moco deficiency.

267 To further test the impact of *cdo-1* on the formation of xanthine stones, we engineered *xdh-1; sulp-*
268 *4; cdo-1* triple mutant *C. elegans*. Surprisingly, *xdh-1; sulp-4; cdo-1* triple mutant animals displayed a 5%
269 xanthine stone penetrance, dramatically reduced when compared to the 98% penetrance displayed by
270 *xdh-1; sulp-4* double mutant animals (**Fig. 5A**). Thus, *cdo-1* was necessary for the formation of xanthine
271 stones displayed by *xdh-1; sulp-4* double mutant animals. Interestingly, we still observe a low penetrance
272 of xanthine stones in *xdh-1; sulp-4; cdo-1* triple mutant *C. elegans* suggesting that *cdo-1* activity is not
273 absolutely required for the formation of xanthine stones but only required for the xanthine stone
274 enhancement caused by *sulp-4* loss of function.

275 *cdo-1* encodes the *C. elegans* cysteine dioxygenase, a critical enzyme in the in sulfur amino acid
276 catabolism pathway that breaks down excess cysteine and methionine (**Fig. 1A**) [8, 31, 32]. To determine
277 if the impact of *cdo-1* on the enhanced xanthine stone formation caused by *sulp-4* inactivation was a result
278 of impaired sulfur amino acid catabolism, we used a *cth-2* mutation which eliminates the activity of *C.*
279 *elegans* cystathionase (**Fig. 1A**). Consistent with our results with *cdo-1* loss of function, we found that *cth-*
280 *2; xdh-1; sulp-4* triple mutant animals also displayed a low 19% penetrance of xanthine stones (**Fig. 5A**).
281 Taken together, these genetic data suggest that sulfur amino acid catabolism is required for the
282 enhancement of xanthine stone accumulation caused by loss of *sulp-4* function.

283 Given that *sulp-4* encodes a sulfate permease, we hypothesized that sulfate accumulation during
284 *sulp-4* loss of function was promoting the formation of xanthine stones. Furthermore, we hypothesized that
285 this sulfate was produced endogenously via CTH-2 and CDO-1. To further test this model, we measured
286 sulfur content in large cultures of wild-type and *sulp-4* mutant *C. elegans* using inductively coupled plasma
287 mass spectrometry (ICP-MS). We did not observe any difference in sulfur content between wild-type and
288 *sulp-4* mutant animals, demonstrating that *sulp-4* mutant *C. elegans* do not accumulate sulfur (**Fig. S5B**).
289 Similarly, we saw no difference in K, Fe, Zn, Mn, Cu or Mo content between wild type and *sulp-4* mutant
290 animals (**Fig. S5**). A key limitation of this method is that ICP-MS does not distinguish between sulfur found
291 in different metabolites such as sulfate, sulfite, methionine, cysteine, etc. Thus, it is plausible that *sulp-4*
292 mutant animals accumulate sulfate with a corresponding decrease in another sulfur-containing metabolite.
293 Alternatively, sulfate sulfur may only account for a small fraction of the animal sulfur economy. Thus,

294 physiologically significant changes in sulfate may be undetectable given the high background of sulfur
295 found in more common metabolites like cysteine or methionine.
296 To further test the relationship between sulfur amino acid catabolism and xanthine stone formation,
297 we supplemented *xdh-1; sulp-4; cdo-1* or *cth-2; xdh-1; sulp-4* triple mutant *C. elegans* with the sulfur-
298 containing amino acid cysteine and assessed the impact on xanthine stone formation. Cysteine
299 supplementation is informative as it is the product of CTH-2 and the substrate for CDO-1 (**Fig. 1A**). We
300 found that cysteine promoted xanthine stone formation in *cth-2; xdh-1; sulp-4* animals, bypassing the
301 requirement for *cth-2.* Alternatively, cysteine did not promote xanthine stones in *xdh-1; sulp-4; cdo-1*
302 mutant animals, demonstrating that *cdo-1* was necessary for cysteine to promote xanthine stone formation
303 (**Fig. 5B**). This result supports our model that endogenous sulfur amino acid catabolism promotes xanthine
304 stone formation. More specifically, these data demonstrate that a cysteine-derived metabolite downstream
305 of CDO-1 is acting to promote xanthine stones. This is consistent with our model that sulfate accumulation
306 during *sulp-4* loss of function promotes xanthine stone accumulation.
307 To test whether mutations in *cth-2* or *cdo-1* would suppress the defects in larval and embryonic
308 development displayed by *sulp-4* mutant animals, we assayed larval and embryonic development in *cth-2;*
309 *sulp-4* and *sulp-4; cdo-1* double mutant animals and compared to *sulp-4* single mutant animals. Consistent
310 with their suppression of xanthine stone formation, *cth-2* or *cdo-1* mutations suppressed the
311 developmental delay and embryonic lethality caused by a *sulp-4* mutation (**Fig. 5C,D**). After 72 hours
312 growth from L1, 0% of *sulp-4* mutant animals reached the young adult stage, 53% reached L4, and 47%
313 failed to reach L4 (n=32). In contrast, 100% of *cth-2; sulp-4* or *sulp-4; cdo-1* double mutant animals
314 reached the young adult stage (n=32) Thus, we conclude that *cth-2* and *cdo-1* are broadly required for
315 phenotypes caused by *sulp-4* loss of function.
316 **Loss of *osm-8* promoted xanthine stone accumulation in *xdh-1* mutant animals, linking osmotic**
317 **homeostasis and xanthine stone formation.**
318 What is the mechanism by which sulfates, derived from CTH-2 and CDO-1, might promote
319 xanthine stone formation when *sulp-4* is inactivated? Given that *sulp-4* encodes a sulfate permease that
320 functions in the *C. elegans* excretory cell, we hypothesized that *sulp-4* mutant animals may be
321 experiencing osmotic imbalance driven by excess sulfate. Supporting this model, *sulp-4* mutant animals
322 accumulated 25% more sodium than their wild-type counterparts as measured by ICP-MS (**Fig. 6A**).
323 These data demonstrate that *sulp-4* mutant animals are experiencing osmotic imbalance.
324 To test the model that osmotic imbalance promotes the formation of xanthine stones, we
325 challenged *xdh-1* mutant animals with supplemental NaCl. Interestingly, *xdh-1* mutant animals were
326 extremely sensitive to high environmental NaCl when compared to wild type, a phenotype also displayed
327 by rats lacking *xdh-1* (**Fig. 6B**) [33]. These data indicate a conserved role for *xdh-1* in promoting
328 hyperosmotic stress tolerance. However, the sensitivity of *xdh-1* mutant *C. elegans* to NaCl limited our
329 ability to directly test whether hyperosmotic stress promotes xanthine stone formation in an *xdh-1* mutant
330 background.

To genetically test whether osmotic imbalance may promote xanthine stones, we used a loss-of-function mutation in *osm-8* that constitutively activates the hyperosmotic stress response in the absence of environmental osmotic stress [15, 34]. *osm-8* encodes a mucin-like protein and is expressed in the *C. elegans* hypodermis [15]. Interestingly, *osm-8; xdh-1* double mutant *C. elegans* developed xanthine stones like *xdh-1; sulp-4* double mutant animals (**Fig. 6C)**. Although, the xanthine stones observed in *osm-8; xdh-1* double mutant animals were not as large as those observed in *xdh-1; sulp-4* animals (**Fig. S1).** Furthermore, like *xdh-1; sulp-4* double mutant *C. elegans*, *cdo-1* was necessary for the formation of xanthine stones in *osm-8; xdh-1* double mutant animals (**Fig. 6C)**. However, it should be noted that *cdo-1* loss of function incompletely suppressed the formation of xanthine stones in *osm-8; xdh-1* mutant animals, suggesting additional pathways downstream of *osm-8* that govern xanthine stone formation. These data suggest that altered osmotic homeostasis, driven by *osm-8* loss of function, is sufficient to cause xanthine stone accumulation when XDH-1 is inactive.

We wondered if *sulp-4* and *osm-8* mutant animals display additional overlapping phenotypes. *osm-8* mutant *C. elegans* are resistant to high NaCl stress and display increased transcription of the hypertonic stress response which includes the key regulators of osmolyte accumulation, *gpdh-1* and *hmit-1.1* [15, 34]. *gpdh-1* encodes glycerol 3-phosphate dehydrogenase and is required to produce glycerol, a critical osmolyte [35, 36]. *hmit-1.1* encodes an H^+/*myo*-inositol transporter and functions to import *myo*-inositol, another important osmolyte [37]. Distinct from *osm-8* mutant animals, *sulp-4* mutant *C. elegans* were not resistant to high NaCl (**Fig. 6B)**. Furthermore, *sulp-4* mutant animals did not significantly accumulate *hmit-1.1* mRNA and modestly accumulated *gpdh-1* mRNA when compared to the wild type **(Fig. S6A,B**). These data suggest that *sulp-4* inactivation does not robustly activate transcription of all canonical hypertonic stress response genes. Interestingly, both *sulp-4* and *osm-8* mutant animals accumulated *cdo-1* mRNA when compared to the wild type (**Fig. 6D**), consistent with previous studies in *C. elegans* and mammals that demonstrate *cdo-1* induction by osmotic imbalance (high NaCl exposure or *osm-8* inactivation) [34, 38]. Taken together, these data highlight overlapping but distinct phenotypic profiles for *sulp-4* and *osm-8* mutant *C. elegans* and elucidate a positive feedback loop connecting *sulp-4,* osmotic imbalance, and *cdo-1* activation.

In addition to its role in cysteine catabolism, CDO-1 is also essential for synthesis of the osmolyte taurine [32, 38]. Given that *cdo-1* was necessary for phenotypes caused by *sulp-4* inactivation, we wondered whether inactivating mutations in other genes involved in osmolyte accumulation may also suppress *sulp-4* mutant phenotypes. To test this, we engineered *gpdh-1; sulp-4* and *hmit-1.1; sulp-4* double mutant strains of *C. elegans* and assayed for the formation of xanthine stones when animals were cultured on a Moco- diet. Unlike *cdo-1,* neither *gpdh-1* nor *hmit-1.1* were necessary for the formation of xanthine stones caused by a *sulp-4* mutation (**Fig. S6C**). These data suggest that the suppression of *sulp-4* mutant phenotypes by *cdo-1* loss-of-function is specific and not a general feature of inactivating mutations in genes involved in osmolyte accumulation.

We propose the model that in healthy wild-type *C. elegans,* cysteine and methionine are being broken down by the sulfur amino acid catabolism pathway (CTH-2/CDO-1), maintaining sulfur homeostasis. This results in the production of sulfate which is exported into the environment via the action of SULP-4 in the excretory cell. However, when *sulp-4* is inactive, sulfate cannot be safely excreted and accumulates. This issue is exacerbated by an induction of *cdo-1* mRNA during *sulp-4* loss of function. This creates a maladaptive positive feedback loop that we anticipate would further increase sulfate production. We speculate that sulfate accumulation then promotes osmotic imbalance which causes embryonic lethality, impaired larval development, and an increased propensity to form xanthine stones when *xdh-1* is inactive (**Fig. 7**).

Discussion:

Modeling xanthinuria in C. elegans.

Human xanthinuria was originally described in 1954, and presents with high urinary xanthine, low uric acid in serum and urine, the formation of xanthine stones, and, in some cases, renal failure [5, 39]. Still, there are no curative treatments for xanthinuria or the formation of xanthine stones. The current recommendation for patients is a high fluid intake and low purine diet [7]. Thus, understanding the cellular mechanisms that regulate the pathology associated with xanthinuria is an important goal.

Animal models, such as *C. elegans,* are powerful tools for exploring the pathology of rare inborn errors of metabolism including NGLY1 deficiency, Moco deficiency, Friedrich's ataxia, and many others [8, 40, 41]. Here we used *C. elegans* to model human type I and type II xanthinuria. We employed genetic strategies to inhibit XDH-1 activity by mutating the *xdh-1* gene (type I) or limiting animal Moco (type II) [4, 5]. Both manipulations recapitulated a critical feature of human XDH deficiency, the formation of insoluble xanthine stones.

Interestingly, xanthine stones are highly autofluorescent and visible with a standard fluorescence microscope, a phenotype that has been previously characterized in the model plant *Arabidopsis thaliana* [18]. Given the transparent nature of *C. elegans,* this phenotype empowers genetic analyses of xanthine stone accumulation and, by proxy, purine biology. Here we used the power of *C. elegans* genetics in combination with this simple phenotype to identify and characterize regulators of purine homeostasis.

Defining genetic regulators of xanthine stone formation.

We sought to define genetic regulators of the formation of xanthine stones. Given the established purine catabolism pathway (**Fig. 1A)**, we used a hypothesis-driven approach to define genes that regulate the formation of xanthine stones. Purine nucleoside phosphorylase (PNP-1/PNP) was a lead candidate given its biochemical requirement for the formation of xanthine. Indeed, we demonstrated that *pnp-1* was necessary for the formation of xanthine stones in our *C. elegans* mutant animals: *pnp-1* loss of function suppressed the formation of xanthine stones in an *xdh-1; sulp-4* double mutant background. These results suggest that inhibiting the activity of PNP may be a therapeutic strategy for limiting the accumulation of xanthine and xanthine stones in patients suffering from xanthinuria. However, this treatment strategy may

404 be fraught, given the consequences of PNP inactivation. Human patients with PNP deficiency display
405 impaired T-cell immunity [3]. In fact, a potent PNP inhibitor has been developed, and induces apoptosis of
406 B- and T-lymphocytes [42, 43]. Thus, the potential benefits of PNP inhibition in the treatment of human
407 xanthinuria patients would need to be evaluated and weighed against the negative impacts on the immune
408 system.

409 To identify new and unexpected regulators of purine homeostasis, we employed an unbiased
410 genetic approach. In a forward genetic screen, we identified *sulp-4* as a potent modifier of xanthine stone
411 formation. Loss-of-function mutations in *sulp-4* dramatically enhanced the penetrance and expressivity of
412 xanthine stone formation in our *C. elegans* models of xanthinuria. Interestingly, we also found that *sulp-4*
413 was necessary for promoting normal larval and embryonic development. These genetic data demonstrate
414 that *sulp-4* promotes healthy development and acts in a parallel pathway to *xdh-1* to limit the accumulation
415 of xanthine stones.

416 *sulp-4* was previously demonstrated to encode a sulfate permease that localizes to the apical
417 membrane of the excretory cell, which we also observed [13]. Importantly, we demonstrated that *Psulp-*
418 *4::SULP-4::GFP* rescued the formation of xanthine stones displayed by an *xdh-1; sulp-4* double mutant
419 animal. This functional rescue is strong evidence that *sulp-4* is acting in the excretory cell to limit the
420 formation of xanthine stones. Interestingly, xanthine stones accumulate in the lumen of the *C. elegans*
421 intestine while *sulp-4* acts in the excretory cell. Thus, we conclude that *sulp-4* acts cell-nonautonomously
422 to limit xanthine stone accumulation. These data establish a new intersection between SULP-4, the
423 excretory cell, and purine homeostasis.

424 *Linking osmotic homeostasis and xanthine stone formation.*

425 We next sought to understand the nature of the genetic interaction between *sulp-4* and *xdh-1* with
426 respect to xanthine stone formation. Given that *sulp-4* encodes a sulfate transporter that acts cell-
427 nonautonomously in the excretory cell, we hypothesized that *sulp-4* mutations may cause sulfate retention
428 and disturb osmotic balance in *C. elegans* systemically [13]. Indeed, we found that *sulp-4* mutant *C.*
429 *elegans* accumulated sodium, demonstrating osmotic imbalance [44, 45]. Importantly, we do not know the
430 site of excess sodium accumulation (cellular vs. extracellular) in *sulp-4* mutant *C. elegans.* We propose the
431 model that osmotic imbalance in *sulp-4* mutant animals is driven by a failure to excrete endogenously
432 produced sulfates. This model is supported by our genetic demonstration that *cth-2* or *cdo-1,* genes that
433 encode enzymes necessary for sulfate production, were necessary for xanthine stone formation in *xdh-1;*
434 *sulp-4* mutant animals. We speculate that osmotic imbalance driven by sulfate retention may promote
435 water reabsorption causing dehydration in the intestinal lumen, increasing xanthine concentration and
436 stone formation. This model is reinforced by our observation that activation of the hyperosmotic stress
437 response through a distinct genetic perturbation, *osm-8* loss of function, also promoted the formation of
438 xanthine stones in an *xdh-1* mutant background [15]. In the case of *osm-8* inactivation, we speculate that
439 glycerol accumulation would drive water reabsorption and dehydration in the intestinal lumen. Again, this
440 dehydration would increase xanthine concentration, promoting stone formation.

441 *Intersection between sulfur amino acid metabolism and Moco-dependent metabolism.*

442 Previous studies in *C. elegans* identified *cth-2* and *cdo-1* loss of function mutations as suppressors
443 of the lethality associated with Moco deficiency and deficiency of the Moco-requiring enzyme sulfite
444 oxidase [8]. Loss of sulfite oxidase is lethal in *C. elegans* and humans due to the accumulation of its
445 reactive and toxic substrate, sulfite (**Fig. 1A**) [8, 46]. *cth-2* and *cdo-1* inactivation limit the accumulation of
446 sulfites, suppressing the lethality caused by Moco or sulfite oxidase deficiency. Is it a coincidence that loss
447 of *cth-2* or *cdo-1* suppress phenotypes associated with two distinct Moco-requiring enzymes; i) lethality
448 displayed by *suox-1* null mutant animals and ii) xanthine stone formation of *xdh-1; sulp-4* double mutant
449 animals? Given that the substrates and products of these two Moco-dependent enzymes are distinct, it is
450 peculiar that loss-of-function phenotypes of both are modulated by these common genetic factors. Future
451 studies are required to tease apart the potential molecular intersections between CTH-2/CDO-1 and these
452 Moco-dependent pathways.

453 An additional layer of complexity is added when considering the regulation of *cdo-1.* Here, we
454 reinforce previous observations that *cdo-1* is activated in response to hyperosmotic stress [34, 38]. *sulp-4*
455 and *osm-8* mutant *C. elegans* both accumulated *cdo-1* mRNA. Yet, CDO-1/CDO levels and activity are
456 also modified by dietary sulfur amino acid content. This regulation includes both transcriptional and post-
457 translational control of cysteine dioxygenase [31, 47-51]. Given that SULP-4 mediates sulfate transport
458 and sulfate is a metabolic product of sulfur amino acid catabolism governed by CTH-2/CDO-1/SUOX-1,
459 sulfate seems like a potential metabolic intersection between these seemingly disparate Moco-dependent
460 pathways. Whether there is any overlap between the mechanisms of CDO-1/CDO regulation downstream
461 of hyperosmotic stress and high sulfur amino acid content remains to be studied.

462 *SULP-4 homologs are implicated in calcium oxalate stone formation.*

463 Our genetic studies demonstrate that SULP-4 plays a role in limiting the formation of xanthine
464 stones in *C. elegans* models of xanthinuria. SULP-4 is homologous to human SLC26 proteins which have
465 been previously linked to metabolic stone formation. Understanding the connection between SLC26
466 proteins, like SULP-4, and the formation of metabolic stones is important as 1 out of every 10 individuals
467 in the United States will develop a kidney stone over the course of their lifetimes [52]. For instance, mouse
468 SLC26A6 limits urolithiasis, paralleling our results with *C. elegans* SULP-4. Specifically, SLC26A6 null
469 mutant mice develop a high incidence of calcium oxalate stones in the bladder [53]. Similarly, a dominant
470 negative mutation in SLC26A6 and loss of function mutations in SLC26A1 are proposed to cause calcium
471 oxalate nephrolithiasis in humans [54, 55]. In contrast, the *Drosophila melanogaster* homolog of human
472 SLC26A5/6, dPrestin, promotes the formation of calcium oxalate stones in the Malpighian tubules in a
473 dietarily-induced model of calcium oxalate nephrolithiasis. Under a diet of high oxalate, *Drosophila*
474 develop calcium oxalate stones whose formation is dampened by RNAi knockdown of dPrestin [56]. With
475 respect to calcium oxalate stones, the mechanism of stone formation is believed to relate directly to the
476 role of the SLC26 family members in oxalate transport. Loss of SLC26 proteins results in higher or lower
477 concentrations of oxalate in a given space, altering the likelihood of stone formation. We propose that

478 xanthine is the critical component of the stones that form in *xdh-1; sulp-4* mutant animals, not oxalate. In
479 heterologous transport assays, oxalate was not meaningfully transported by SULP-4 [13]. However, it is
480 possible that *sulp-4* mutations may enhance the formation of additional metabolic stones given a specific
481 genetic or environmental perturbation. This hypothesis remains to be tested. Regardless, we think it is
482 very intriguing that SLC26 homologs in mouse, humans, flies, and worms have all been shown to play
483 roles in metabolic stone formation and suggest the potential for a fundamental mechanism underlying
484 these discrete observations.
485
486 **Materials and methods:**
487 General methods and strains:
488 *C. elegans* were cultured using established protocols [22]. Briefly, animals were cultured at 20°C
489 on nematode growth media (NGM) seeded with wild-type *E. coli* (OP50) unless otherwise noted. The wild-
490 type strain of *C. elegans* was Bristol N2. Additional *E. coli* strains used in this work were BW25113 (Wild
491 type, Moco+) and JW0764-2 (Δ*moaA753::kan,* Moco-) [57].
492 *C. elegans* mutant and transgenic strains used in this work are listed here. When previously
493 published, sources of strains are referenced. Unless a reference is provided, all strains were generated in
494 this study.
495 **Non-transgenic strains:**
496 N2, wild type [22]
497 GR2257, *cth-2(mg599) II* [8]
498 GR2259, *cth-2(mg599) II; moc-1(ok366) X* [8]
499 GR2260, *cdo-1(mg622)* [8]
500 GR2261, *cdo-1(mg622) moc-1(ok366) X* [8]
501 USD869, *xdh-1(ok3234) IV* (Outcrossed 2X)
502 USD1033, *sulp-4(rae319) V* (Outcrossed 4X)
503 USD1037, *sulp-4(rae319) V; cdo-1(mg622) moc-1(ok366) X*
504 USD1038, *sulp-4(rae319) V; cdo-1(mg622) X*
505 USD1055, *xdh-1(ok3234) IV; sulp-4(rae334) V*
506 USD1091, *sulp-4(rae334) V; cdo-1(mg622) X*
507 USD1103, *cth-2(mg599) II; sulp-4(rae334) V*
508 USD1105, *cth-2(mg599) II; xdh-1(ok3234) IV; sulp-4(rae334) V*
509 USD1146, *xdh-1(ok3234) IV; sulp-4(rae334) V; cdo-1(mg622) X*
510 USD1154, *xdh-1(ok3234) IV; cdo-1(mg622) X*
511 USD1163, *pnp-1(jy121) IV* (Outcrossed 1X) [25]
512 USD1170, *cth-2(mg599) II; xdh-1(ok3234) IV*
513 USD1174, *pnp-1(jy121) xdh-1(ok3234) IV*
514 USD1198, *pnp-1(jy121) IV; sulp-4(rae319) V*

515 USD1215, *pnp-1(jy121) xdh-1(ok3234) IV; sulp-4(rae319) V*
516 USD1230, *aex-5(sa23) I; xdh-1(ok3234) IV*
517 USD1269, *exc-5(rh232) xdh-1(ok3234) IV*
518 USD1308, *osm-8(n1518) II; xdh-1(ok3234) IV*
519 USD1310, *gpdh-1(ok1558) I* (Outcrossed 4X)
520 USD1312, *hmit-1.1(ok2923) V* (Outcrossed 4X)
521 USD1322, *gpdh-1(ok1558) I; sulp-4(rae319) V*
522 USD1324, *sulp-4(rae319) hmit-1.1(ok2923) V*
523 USD1327, *osm-8(n1518) II; xdh-1(ok3234) IV; cdo-1(mg622) X*
524 JT23, *aex-5(sa23) I [30]*
525 NJ731, *exc-5(rh232) IV* [28]
526 MT3571, *osm-8(n1518) II* [15]
527 RB1082, *sulp-5(ok1048) V*
528 RB1366, *sulp-2(ok1551) X*
529 RB1369, *sulp-2(ok1554) X*
530 RB1436, *sulp-1(ok1639) I*
531 RB2134, *sulp-8(ok2842) V*
532 FX08263, *sulp-5(tm8264) X*
533 VC3021, *sulp-7(ok3751) X*
534 VC3045, *sulp-7(ok3752) X*
535 **Transgenic strains:**
536 USD1060, *xdh-1(ok3234) IV; sulp-4(rae319) V; raeEx118*
537 USD1061, *xdh-1(ok3234) IV; sulp-4(rae319) V; raeEx119*
538 USD1062, *xdh-1(ok3234) IV; sulp-4(rae319) V; raeEx120*
539 USD1251, *qpIs11 I; sulp-4(rae319) V*
540 USD1277, *qpIs11 I; exc-5(rh232) IV*
541 BK36, *qpIs11 I; unc-119(ed3) III* [58]
542 **EMS-derived strains:**
543 USD962*, *xdh-1(ok3234) IV; sulp-4(rae299) V*
544 USD1007, *xdh-1(ok3234) IV; sulp-4(rae299) V* (Outcrossed 2X)
545 USD971*, *xdh-1(ok3234) IV; sulp-4(rae302) V*
546 USD997, *xdh-1(ok3234) IV; sulp-4(rae302) V* (Outcrossed 1X)
547 USD990*, *xdh-1(ok3234) IV; sulp-4(rae319) V*
548 USD1001, *xdh-1(ok3234) IV; sulp-4(rae319) V* (Outcrossed 1X)
549 USD1013*, *xdh-1(ok3234) IV; sulp-4(rae320) V*
550 USD1019*, *xdh-1(ok3234) IV; sulp-4(rae326) V*

551 *Whole genome sequencing data for these *C. elegans* strains have been deposited at the NIH Sequence
552 Read Archive (SRA) under accession PRJNA1208078.
553 **CRIPSR/Cas9-derived stains:**
554 USD1042, *sulp-4(rae334) V*
555 Chemical mutagenesis and whole genome sequencing:
556 To define *C. elegans* gene activities that were necessary for promoting purine homeostasis, we
557 carried out a chemical mutagenesis screen for mutations that enhanced the penetrance of xanthine stone
558 formation in *xdh-1(ok3234)* mutant *C. elegans* (USD869). *C. elegans* were mutagenized with ethyl
559 methanesulfonate (EMS) using established protocols [22]. Over multiple rounds of mutagenesis, we
560 surveyed ~100,000 mutagenized haploid genomes. To increase the likelihood of identifying a mutation that
561 enhanced xanthine stone formation, we cloned ~600 F2 generation animals that displayed a xanthine
562 stone onto individual NGM petri dishes. F3 generation animals from these ~600 isolates were then
563 screened qualitatively for a population-level increase in xanthine stone penetrance. We demanded that
564 new mutant strains of interest were viable and fertile.
565 Here we report the analysis of 5 new mutant strains (USD962, USD971, USD990, USD1013, and
566 USD1019). Each of these strains carried new EMS-induced lesions (*rae299, rae302, rae319, rae320,* or
567 *rae326)* that enhanced the formation of xanthine stones in an *xdh-1* mutant background. Each mutation
568 was recessive; when heterozygous, each lesion caused 5% (*rae302, n*=42 individuals), 0% (*rae319, n*=38
569 individuals), 2% (*rae299, n*=41 individuals), or 5% (*rae326, n*=22 individuals) xanthine stone formation in
570 an *xdh-1* mutant background, dramatically reduced when compared to their homozygous counterparts
571 (**Fig. 2B)**. *rae320* was never characterized as dominant or recessive.
572 To further genetically analyze these lesions, we performed complementation analyses of these new
573 mutations. The *rae319* lesion failed to complement *rae302* (100% xanthine stone penetrance, *n*=71
574 individuals), *rae299* (87% xanthine stone penetrance, *n*=38 individuals), and *rae326* (100% xanthine stone
575 penetrance, *n*=14 individuals). All complementation experiments were performed in an *xdh-1(ok3234)*
576 homozygous mutant genetic background. These results suggest *rae302, rae319, rae299,* and *rae326* all
577 impact the same gene. Complementation studies were not performed on *rae320.*
578 To identify EMS-induced mutations in our strains of interest we followed established protocols [59].
579 Briefly, whole genomic DNA was prepared from *C. elegans* using the Gentra Puregene Tissue Kit (Qiagen)
580 and genomic DNA libraries were prepared using the NEBNext genomic DNA library construction kit (New
581 England Biolabs). DNA libraries were sequenced on an Illumina NovaSeq and deep sequencing reads
582 were analyzed using standard methods on Galaxy, a web-based platform for computational analyses [60].
583 Briefly, sequencing reads were trimmed and aligned to the WBcel235 *C. elegans* reference genome [61,
584 62]. Variations from the reference genome and the putative impact of those variations were annotated and
585 extracted for analysis [63-65]. All 4 strains that formed a complementation group possessed novel
586 mutations in the gene *sulp-4,* strongly suggesting that these lesions in *sulp-4* caused the enhanced
587 xanthine stone formation in the *xdh-1* mutant background (**Fig. 2A, Table S1**). Although the *rae320* lesion

588 found in USD1013 was not analyzed via complementation, whole genome sequence analyses identified a
589 homozygous mutation in *sulp-4*. Thus, we assume that the lesion in *sulp-4* found in USD1013 is also
590 causative for the enhanced xanthine stone formation in the *xdh-1* mutant background (**Table S1)**. In fact,
591 *rae319* and *rae320* are identical genetic lesions. We know that strains carrying these genetic lesions are
592 not siblings as they were derived from independent rounds of mutagenesis. Whole genome sequencing
593 data for these *C. elegans* strains have been deposited at the NIH Sequence Read Archive (SRA) under
594 accession PRJNA1208078.
595 CRISPR/Cas9 genome editing:
596 Genome engineering using CRISPR/Cas9 technology was performed using established techniques
597 [23, 24]. Briefly, 2 guide RNAs were designed and synthesized (IDT, crRNA) that targeted the *sulp-4* locus
598 (5'-agagttagctttgtacaacg-3' and 5'-atagcacatgatacttccgt-3'). Cas9 (IDT) guide RNA ribonucleoprotein
599 complexes were directly injected into the *C. elegans* germline [23]. Newly induced deletions were
600 identified in the offspring of injected animals using a PCR-based screening approach. The DNA primers
601 used to screen for new deletions were: 5'-gcagagaaactcagagcaacaa-3' and 5'- gcttggtttggaaactttgg-3'. We
602 were able to isolate and homozygoze *sulp-4(rae334),* a new deletion of *sulp-4* (**Fig. 2A**).
603 *C. elegans* transgenesis:
604 Transgenic *C. elegans* carrying extrachromosomal arrays were generated by micro-injecting the
605 gonad of young adult *xdh-1(ok3234); sulp-4(rae319)* double mutant *C. elegans* with an injection mix
606 consisting of the *Psulp-4::SULP-4::GFP* plasmid (20 ng/μl), the *Pmyo-2::mCherry* co-injection marker (2
607 ng/μl), and the KB+ ladder (78 ng/μl, New England Biolabs) [66]. Three independently derived transgenic
608 strains carrying the extrachromosomal arrays *raeEx118, raeEx119,* or *raeEx120* were isolated and
609 maintained by propagating individual animals based on expression of the fluorescent mCherry protein in
610 the pharynx.
611 Determination of xanthine stone penetrance:
612 To determine the percentage of animals that developed a xanthine stone, we cultured wild-type,
613 mutant, and transgenic *C. elegans* beginning at the L1 stage of development under various growth
614 conditions. Animals were assessed for the formation of a xanthine stone beginning at the L4 stage.
615 Animals were assessed daily through the first 4 days of adulthood except for experiments that used the
616 *cdo-1(mg622)* allele or supplemental cysteine where assays were terminated at day 3 or 2 of adulthood
617 respectively. *cdo-1(mg622)* and supplemental cysteine caused early lethality that limited the number of
618 individuals that survived per biological replicate. Thus, the assays were shortened to increase the sample
619 size in **Fig. 1B, 5A, 5B, 6C, and S4**. Importantly, all datapoints in a given figure panel were subjected to
620 the same assay conditions and are thus directly comparable. Xanthine stones were determined based
621 upon presence of exceptionally bright autofluorescent puncta that were opaque when observed by
622 brightfield microscopy. If an individual displayed a stone, it was scored as such and removed from the
623 assay. If an animal did not display a stone, it was counted and moved to a fresh petri dish to prevent
624 contamination from the subsequent generation and allow for assessment on the following day. Thus, if an

625 animal displayed a xanthine stone on any day of the assay, it scored positive and counted towards the
626 penetrance of the phenotype. Xanthine stone penetrance was the percentage of animals that displayed a
627 stone over the course of the assay. If animals went missing or died before the end of the assay, they were
628 not included in the final analyses.

629 *C. elegans* larval development and embryonic viability assays:

630 To assay developmental rates, *C. elegans* were synchronized at the first stage of larval
631 development. To synchronize animals, embryos were harvested from gravid adult animals via treatment
632 with a bleach and sodium hydroxide solution. Embryos were then incubated overnight in M9 solution
633 causing them to hatch and arrest development at the L1 stage [67]. Synchronized L1 animals were
634 cultured for 72 hours under standard conditions, and live animals were imaged as described below. Animal
635 length was measured from tip of head to the end of the tail.

636 To determine the hatching rate of wild-type and mutant *C. elegans,* we performed synchronized
637 egg lays using young adult animals. Embryos were then scored for hatching ~24 hours after being laid.

638 Microscopy:

639 Low magnification bright field and fluorescence images (**Fig. 1C and S1**) were collected using a
640 Nikon SMZ25 microscope equipped with a Hamamatsu Orca flash 4.0 digital camera using NIS-Elements
641 software (Nikon). High magnification differential interference contrast (DIC) and GFP fluorescence images
642 (**Fig. 2C, 4A,B, and S3B-D**) were collected using a Nikon NiE microscope equipped with a Hamamatsu
643 Orca flash 4.0 digital camera using NIS-Elements software (Nikon). Xanthine stones were visualized and
644 imaged using the EGFP BP (FITC/Cy2) HC Filter Set (Nikon). All images were processed and analyzed
645 using ImageJ software (NIH). All imaging was performed on live animals paralyzed using sodium azide.

646 Quantitative PCR (qPCR):

647 RNA was extracted from synchronized wild-type, *sulp-4(rae319),* and *osm-8(n1518)* young adult
648 animals using Trizol Reagent per manufacturer's instructions (Invitrogen). Prior to RNA extraction, live *C.*
649 *elegans* samples were washed and subsequently incubated for one hour in buffer M9 to allow for removal
650 of bacterial contamination. cDNA was then synthesized using the GoScript Reverse Transcriptase System
651 following manufacturer's instructions (Promega). qPCR was performed using a CFX96 Real-Time System
652 (Bio-Rad) and SYBR Green Master Mix following manufacturer's instructions (Applied Biosystems).
653 Relative mRNA levels were calculated using the comparative C_T methods [68]. Forward and reverse
654 amplification primers were *act-1,* 5'-ctcttgccccatcaaccatg-3' and 5'-cttgcttggagatccacatc-3'; *cdo-1,* 5'-
655 ttcgatgagagaaccggaaag-3' and 5'-gccattcttagatcctctgtagtc-3'; *hmit-1.1,* 5'-ccattgaagaggtagaaatgc-3' and
656 5'-tgtacttcattgtgttgtcc-3'; and *gpdh-1,* 5'-tgcagagattccaggaaaccagg-3' and 5'-ccctttttgtagcttgccacggag-3'.

657 Elemental analyses:

658 For elemental analyses (S, K, Na, Mn, Fe, Cu, Zn, and Mo) of wild-type or *sulp-4(rae319)* mutant
659 *C. elegans,* 29.9 to 34.7 mg of tissue (approximately 20,000 freeze-dried young adult *C. elegans*) were
660 digested in 200μl of concentrated HNO_3 at 90°C for one hour. After digestion, samples were diluted to a
661 working volume of 1.4ml and subsequently diluted an additional 5X (Mn, Fe, Cu, Zn, and Mo) or 200X (S,

662 K, and Na) to produce final samples for elemental analysis. All dilutions were performed with 1% HNO_3.
663 Inductively coupled plasma mass spectroscopy (ICP-MS) analysis was performed using an Agilent 8900
664 triple quad equipped with an SPS autosampler. The system was operated at a radio frequency power of
665 1550 W, an argon plasma gas flow rate of 15 L/min, and an Ar carrier gas flow rate of 0.9 L/min. Data
666 were quantified using weighed, serial dilutions of a multi-element standard (CEM 2, (VHG Labs, VHG-
667 SM70B-100) K, Na, Mn, Fe, Cu, Zn) and a single element standards for S (Spex CertiPrep, PLS9-2M) and
668 Mo (Spex CertiPrep, CLMO9-2Y).
669 NaCl tolerance assay:
670 To assay NaCl tolerance, wild-type, *xdh-1, sulp-4,* or *osm-8* mutant *C. elegans* were synchronized
671 at the first stage of larval development. To synchronize animals, embryos were harvested from gravid
672 adult animals via treatment with a bleach and sodium hydroxide solution. Embryos were then incubated
673 overnight in M9 solution causing them to hatch and arrest development at the L1 stage [67]. Synchronized
674 L1 animals were cultured under standard conditions for 72 hours or until reaching the young adult stage.
675 Young adult animals were then transferred to NGM plates with various NaCl concentrations (50, 200, 300,
676 400, 500, or 600mM NaCl). Animals were scored as alive or dead based on touch responsiveness after a
677 24-hour exposure to the various NaCl conditions. If animals went missing before the end of the assay,
678 they were not included in the final analyses.
679
680 **Acknowledgements:**
681 Some *C. elegans* strains were provided by the CGC, which is funded by the NIH Office of
682 Research Infrastructure Programs (P40 OD010440). We thank the lab of Emily Troemel for providing a *C.*
683 *elegans* strain carrying the *pnp-1(jy121)* mutation. We thank the lab of Keith Nehrke for providing the
684 *Psulp-4::SULP-4::GFP* plasmid (pTS1). Research reported in this publication was supported by the
685 National Institute of General Medical Sciences of the National Institutes of Health under award number
686 R35GM146871 (to K.W.). A.V.A. was supported by the National Science Foundation Division of Biological
687 Infrastructure under award number 1756912. C.B. was supported by the National Institute of Childhood
688 Health and Human Development of the National Institutes of Health under award number R25HD097633.
689 ICP-MS measurements were performed in the OHSU Elemental Analysis Core with partial support from
690 NIH (S10OD028492).
691
692
693
694
695
696
697
698

699 **Figures:**

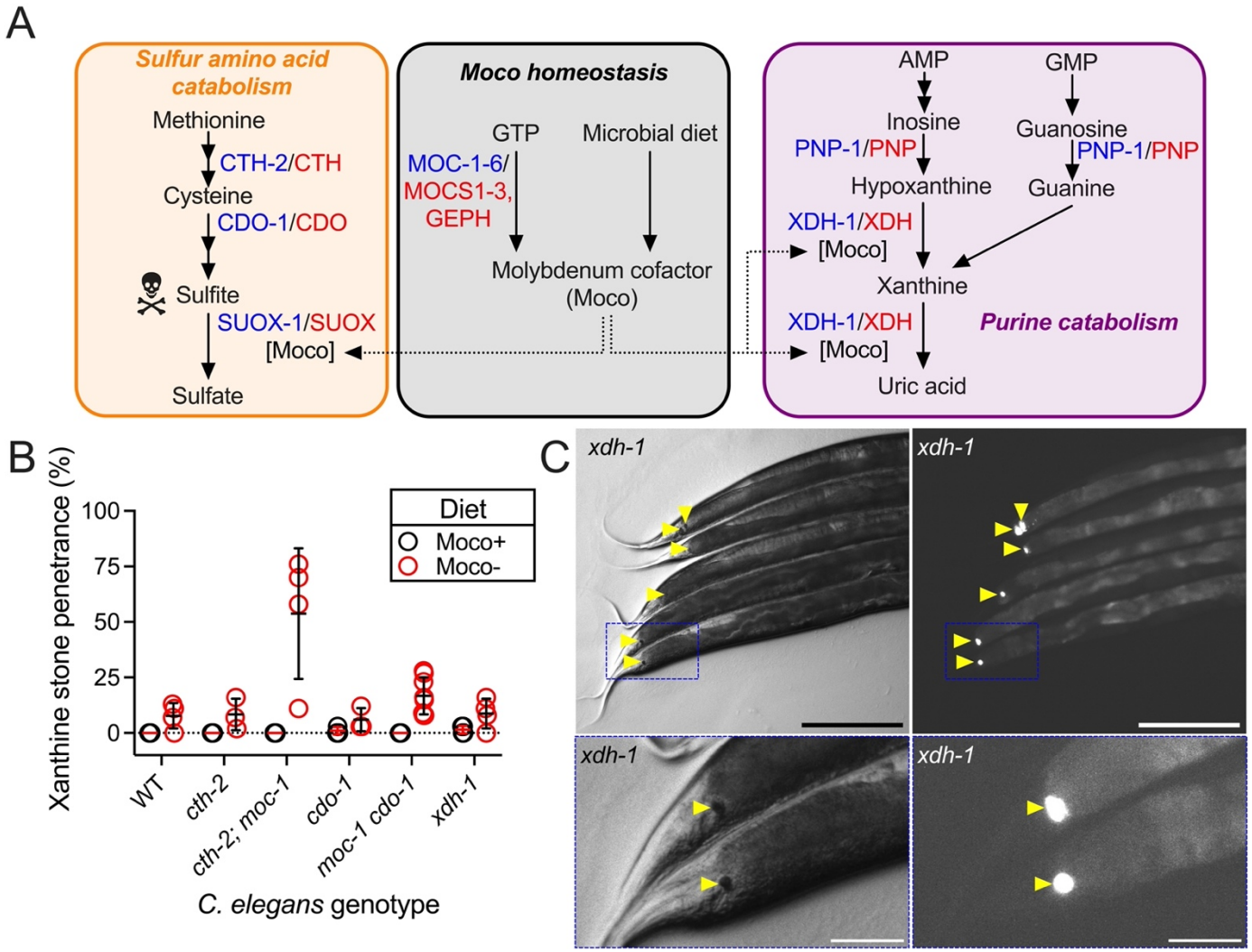

700

701 **Figure 1:** Moco deficiency or loss of *xdh-1* promoted the formation of autofluorescent xanthine stones.
702 A) The role of Moco in *C. elegans* metabolism. We highlight i) pathways for Moco synthesis and import, ii)
703 sulfur amino acid catabolism governed by cystathionase (CTH-2/CTH), cysteine dioxygenase (CDO-
704 1/CDO), and Moco-requiring sulfite oxidase (SUOX-1/SUOX), and iii) purine catabolism controlled by
705 purine nucleoside phosphorylase (PNP-1/PNP) and the Moco-requiring xanthine dehydrogenase (XDH-
706 1/XDH). *C. elegans* enzymes (blue) and their human homologs (red) are displayed. B) Wild-type and
707 mutant *C. elegans* were cultured on wild-type (black, Moco+) or *ΔmoaA* mutant (red, Moco-) *E. coli* and
708 assessed for the formation of xanthine stones over the first 3 days of adulthood. Individual data points
709 represent biological replicates. Mean and standard deviation are displayed. Complete information
710 regarding sample size and individuals scored per biological replicate are found in **Table S2**. C) Brightfield
711 (left) and fluorescent (right) images of the posterior of *xdh-1(ok3234)* mutant adult *C. elegans* cultured on
712 wild-type *E. coli.* Xanthine stones are highlighted (yellow arrowheads). The blue box indicates the region
713 magnified in the lower panels. Scale bar is 250μm (top) or 50μm (bottom).

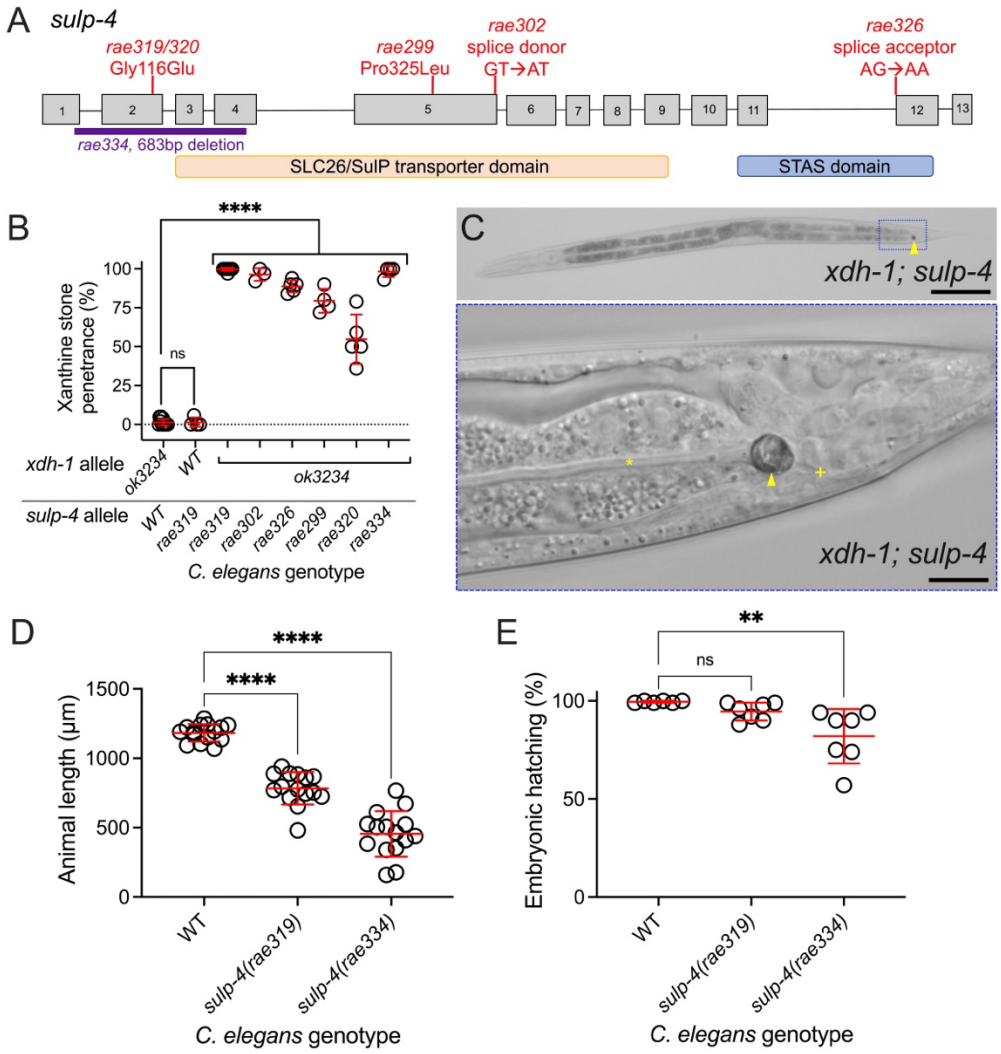

Figure 2: Loss-of-function mutations in *sulp-4* enhanced the formation of xanthine stones during *xdh-1* deficiency.

A) *sulp-4* locus. Gray boxes are exons and lines are introns. The regions that encode the SLC26/SulP sulfate permease domain (orange) and STAS domain (blue) are displayed. Red lines display the location of new EMS-induced lesions that enhanced the formation of xanthine stones in an *xdh-1(ok3234)* mutant background. *rae334* (purple) is a deletion allele generated using CRISPR/Cas9 technology. B) Xanthine stone formation was assessed for *sulp-4(rae319)* single mutant and *xdh-1(ok3234)* mutant *C. elegans* with wild-type (WT) or mutant *sulp-4(rae319, rae302, rae326, rae299, rae320,* or *rae334).* ****, $p<0.0001$, ns, $p>0.05$, ordinary one-way ANOVA. Individual data points represent biological replicates. Mean and standard deviation are displayed. Complete information regarding sample size and individuals scored per biological replicate are found in **Table S2**. C) Differential interference contrast image of *xdh-1(ok3234); sulp-4(rae319) C. elegans* at the L4 stage of development. Blue box indicates the region magnified in the lower panel. Yellow arrowhead identifies the xanthine stone. Yellow asterisk identifies the lumen of the intestine. Yellow plus sign identifies the rectum. Scale bars are 100µm (top) and 10µm (bottom). D) Wild-type, *sulp-4(rae319),* and *sulp-4(rae334)* mutant *C. elegans* were synchronized at the first stage of larval

730 development and cultured for 72 hours on wild-type *E. coli.* Animal length was determined. Individual
731 datapoints are displayed as are the mean and standard deviation. The sample size is 15 individuals per
732 genotype. ****, p<0.0001, ordinary one-way ANOVA. E) The hatching rate of newly laid wild-type, *sulp-*
733 *4(rae319),* and *sulp-4(rae334)* mutant *C. elegans* embryos was determined. Individual data points
734 represent biological replicates. Mean and standard deviation are displayed. Complete information
735 regarding sample size and individuals scored per biological replicate are found in **Table S2**. **, p<0.01 or
736 ns, p>0.05, ordinary one-way ANOVA.

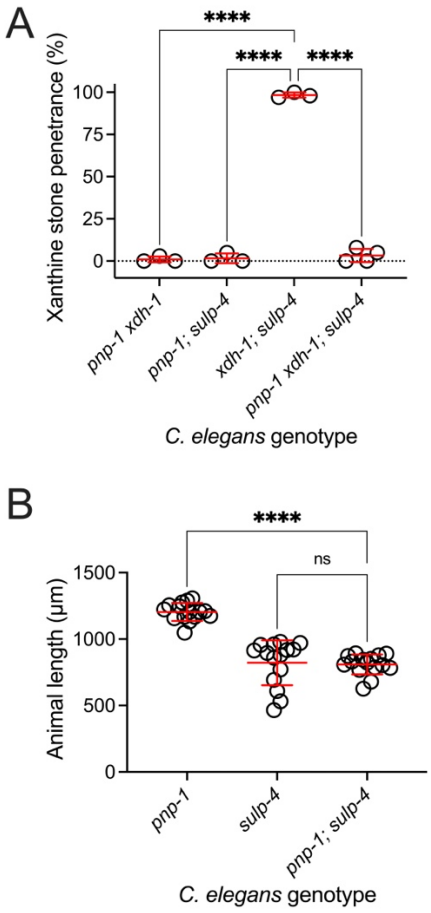

737

738 **Figure 3:** *pnp-1* was required for xanthine stone formation displayed by *xdh-1; sulp-4* mutants but not the
739 larval delay caused by *sulp-4* loss of function.
740 A) Double and triple mutant *C. elegans* were assessed for xanthine stone formation when cultured on wild-
741 type *E. coli*. ****, p<0.0001, ordinary one-way ANOVA. Individual data points represent biological
742 replicates. Mean and standard deviation are displayed. Complete information regarding sample size and
743 individuals scored per biological replicate are found in **Table S2**. B) *pnp-1(jy121), sulp-4(rae319),* and *pnp-*
744 *1(jy121); sulp-4(rae319)* mutant *C. elegans* were synchronized at the first stage of larval development and
745 cultured for 72 hours on wild-type *E. coli.* Animal length was determined. Individual datapoints are
746 displayed as are the mean and standard deviation. The sample size is 15 individuals per genotype. ****,
747 p<0.0001 or ns, p>0.05, ordinary one-way ANOVA.

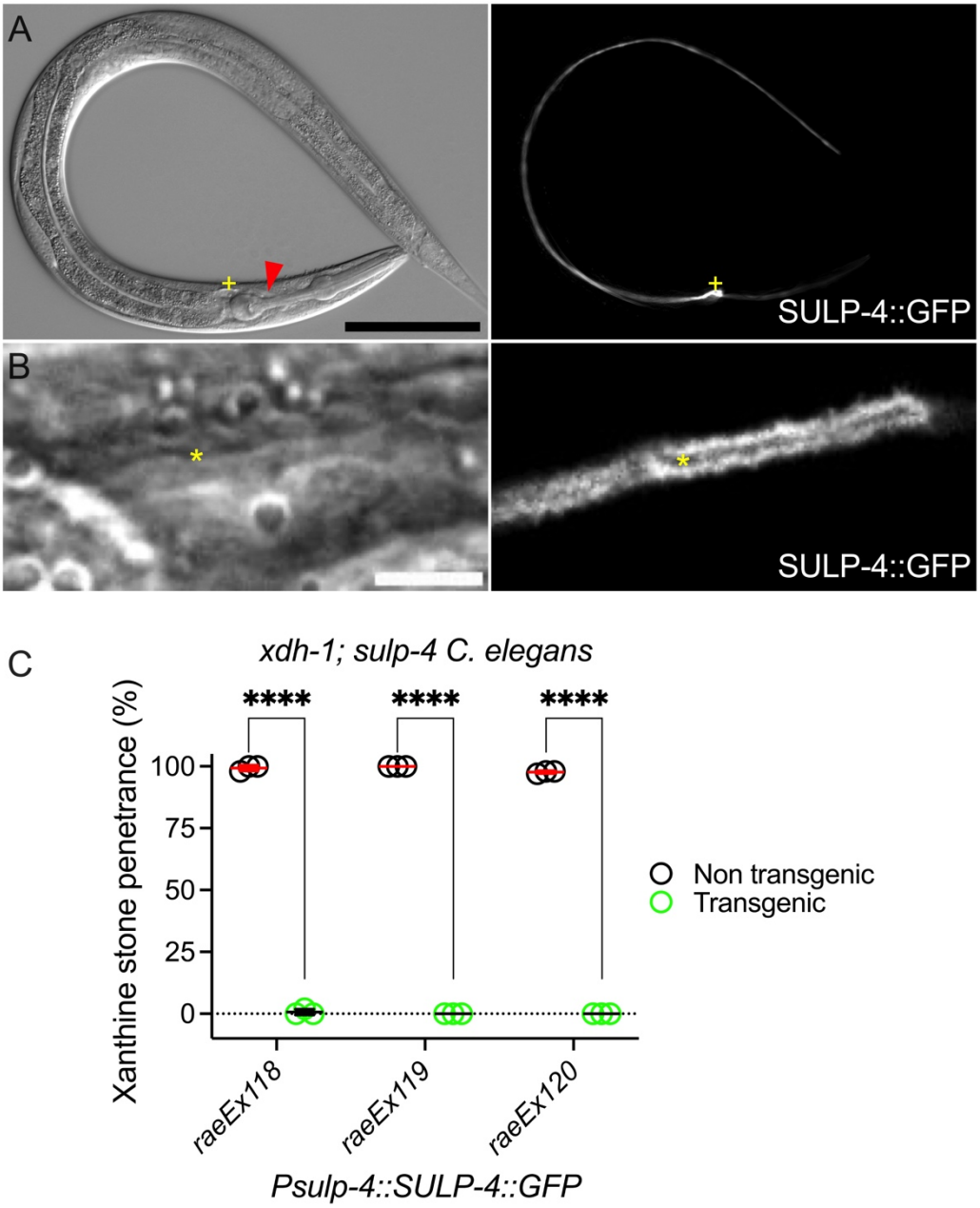

Figure 4: *sulp-4* acted cell non-autonomously in the excretory cell to limit xanthine stone formation. A,B) Differential interference contrast (left) and fluorescence imaging (right) of *xdh-1(ok3234); sulp-4(rae319) C. elegans* expressing the *Psulp-4::SULP-4::GFP* transgene (SULP-4::GFP). Yellow plus sign identifies the cell body of the excretory cell. Red arrow indicates the region magnified in panel B. Yellow asterisk identifies the lumen of the excretory cell. Scale bars are 100μm (A, top) and 5μm (B, bottom). C) Transgenic *xdh-1(ok3234); sulp-4(rae319) C. elegans* expressing the *Psulp-4::SULP-4::GFP* transgene (green) and their non-transgenic siblings (black) were assessed for the formation of xanthine stones. Individual data points represent biological replicates. Mean and standard deviation are displayed. ****, $p<0.0001$, multiple unpaired t tests. Complete information regarding sample size and individuals scored per biological replicate are found in **Table S2**.

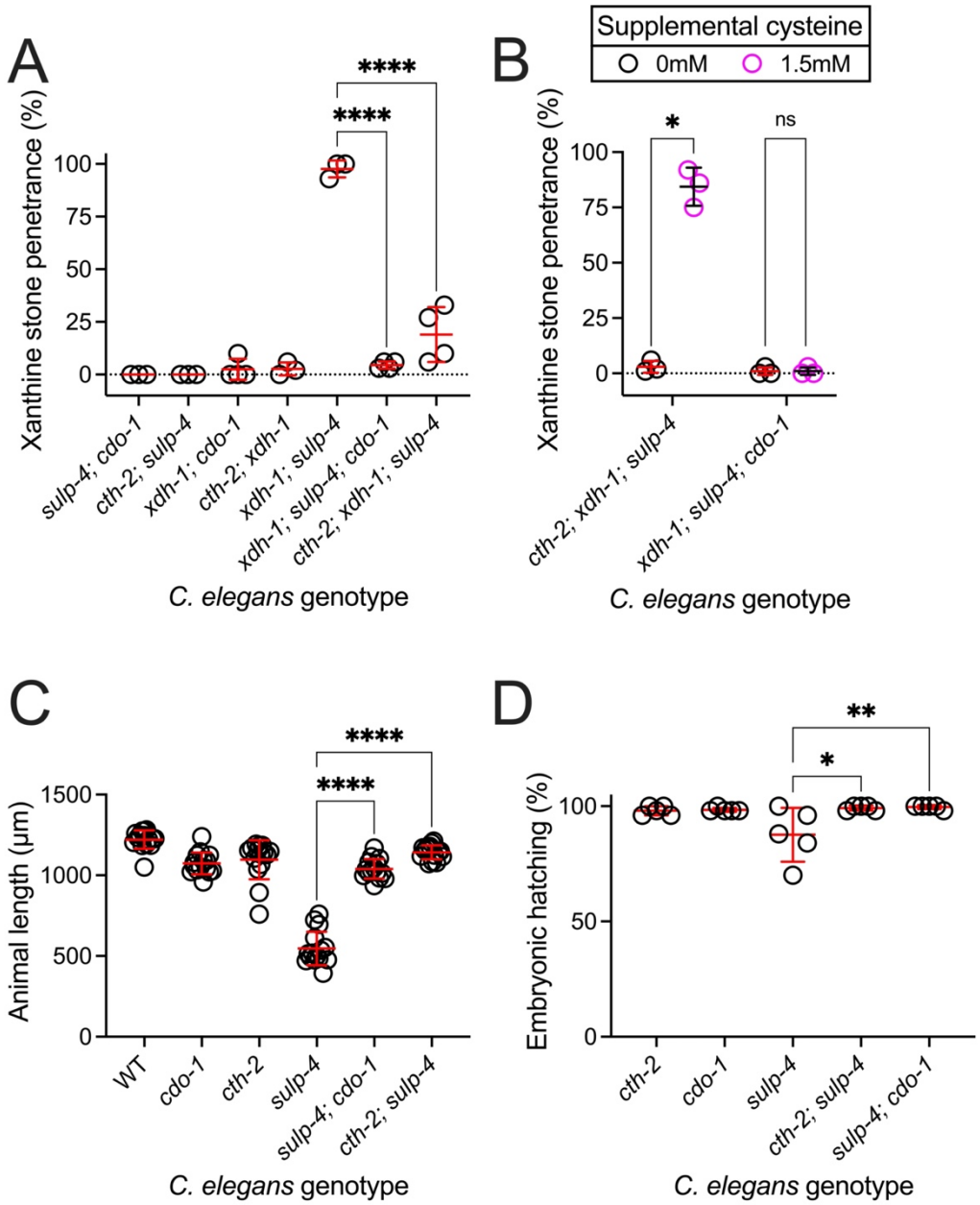

Figure 5: *cth-2* and *cdo-1* were required for phenotypes caused by *sulp-4* loss of function. A) Double and triple mutant *C. elegans* were assessed for xanthine stone formation when cultured on wild-type *E. coli* over the first 3 days of adulthood. Individual data points represent biological replicates. Mean and standard deviation are displayed. ****, $p<0.0001$, ordinary one-way ANOVA. Complete information regarding sample size and individuals scored per biological replicate are found in **Table S2**. B) Triple mutant *C. elegans* exposed to 0 or 1.5mM supplemental cysteine were assessed for xanthine stone formation when cultured on wild-type *E. coli* over the first 2 days of adulthood. Mean and standard deviation are displayed. *, $p<0.05$ and ns, $p>0.05$, multiple unpaired t tests. Complete information regarding sample size and individuals scored per biological replicate are found in **Table S2**. C) Wild-type and mutant *C. elegans* were synchronized at the first stage of larval development and cultured for 72 hours on wild-type *E. coli.* Animal length was determined. Individual datapoints are displayed as are the

mean and standard deviation. The sample size is 15 individuals per genotype. ****, p<0.0001, ordinary one-way ANOVA. D) The hatching rate of newly laid single and double mutant *C. elegans* embryos was determined. Individual data points represent biological replicates. Mean and standard deviation are displayed. **, p<0.01 or *, p<0.05, ordinary one-way ANOVA. Complete information regarding sample size and individuals scored per biological replicate are found in **Table S2**. The *sulp-4(rae334)* allele was used to generate the data in **Fig. 5.**

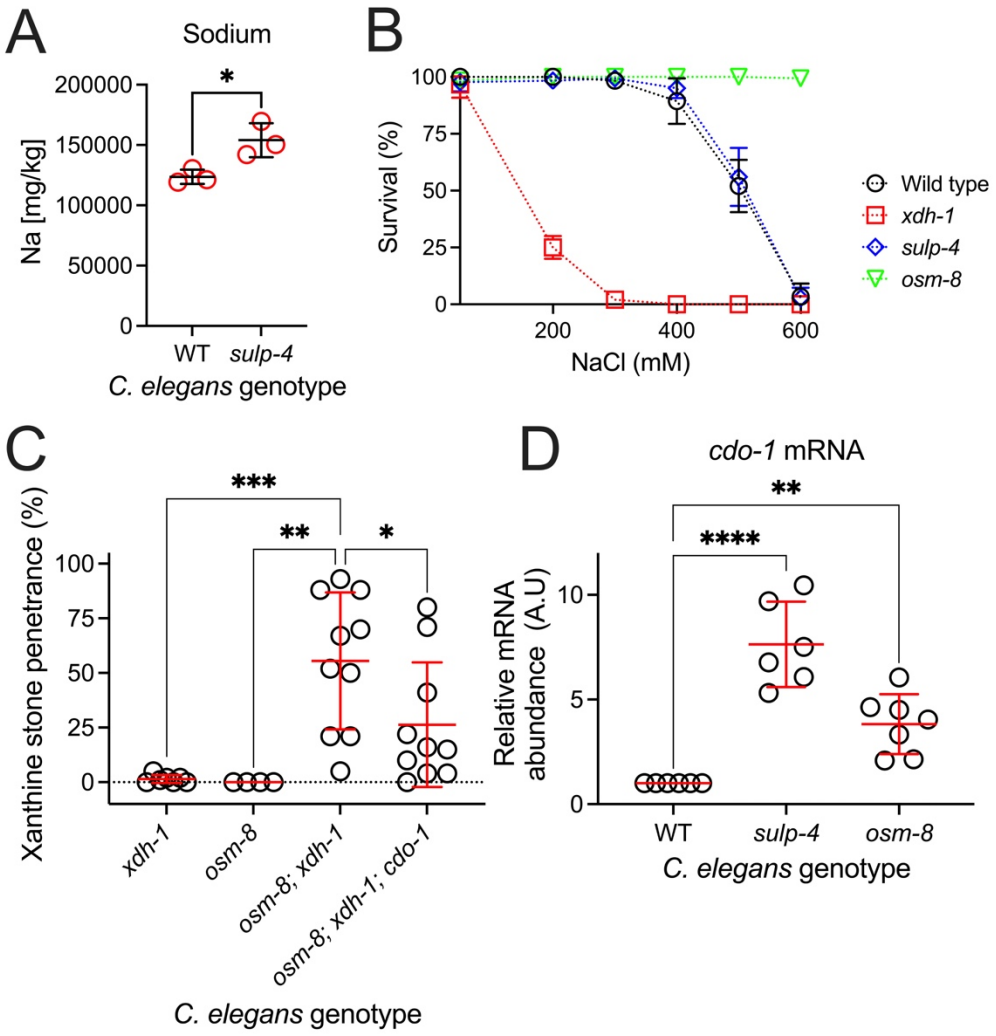

Figure 6: Loss of *osm-8,* which activates the osmotic stress response, enhanced xanthine stone accumulation in *xdh-1* mutant *C. elegans.*

A) Sodium content was determined for synchronized wild-type and *sulp-4(rae319)* young adult *C. elegans* using ICP-MS. Individual data points represent biological replicates. Mean and standard deviation are displayed. *, p<0.05, t test. B) Survival of wild-type, *sulp-4(rae319), xdh-1(ok3234),* or *osm-8(n1518)* young adult *C. elegans* was determined after 24-hour exposure to NGM media containing various concentrations of NaCl. Mean and standard deviation of 3 biological replicates are displayed. Complete information regarding sample size and individuals scored per biological replicate are found in **Table S2**. C) Mutant *C. elegans* were assessed for xanthine stone formation when cultured on wild-type *E. coli*. Individual data points represent biological replicates. Mean and standard deviation are displayed. ***,

p<0.001, **, p<0.01, *, p<0.05, ordinary one-way ANOVA. Complete information regarding sample size and individuals scored per biological replicate are found in **Table S2**. D) Relative mRNA levels of *cdo-1* are displayed for RNA isolated from wild-type, *sulp-4(rae319)*, and *osm-8(n1518)* young adult *C. elegans.* Relative mRNA abundance was determined via the delta-delta C_T method. All transcripts are normalized to *act-1.* Relative mRNA abundance for each transcript was set to one in the wild type. ****, p<0.0001, **, p<0.01, ordinary one-way ANOVA.

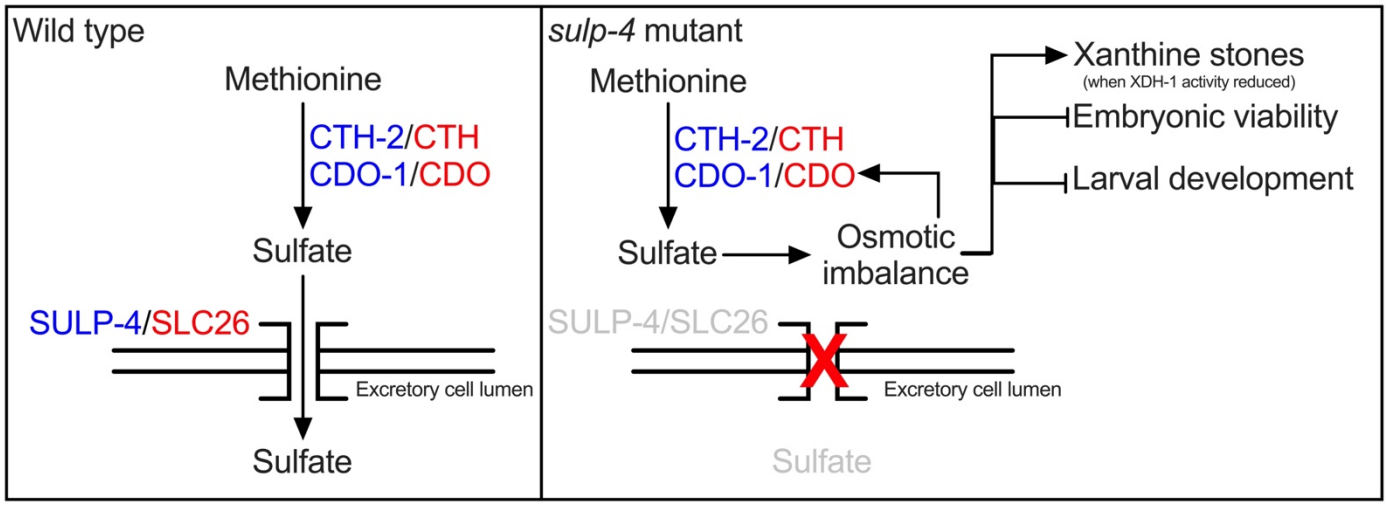

Figure 7: SULP-4 promotes sulfate homeostasis, maintaining osmotic balance in *C. elegans.* In wild-type *C. elegans*, sulfur amino acid catabolism gives rise to sulfate which is maintained at homeostatic levels by SULP-4-mediated exchange with the environment via the excretory cell. During *sulp-4* loss of function, CTH-2/CDO-1-derived sulfates accumulate causing osmotic imbalance. This osmotic imbalance promotes a maladaptive positive feedback loop promoting additional *cdo-1* mRNA accumulation. This cascade culminates in embryonic lethality, altered larval development, and a propensity to form xanthine stones when XDH-1 activity is compromised.

References:

1. Mullen NJ, Singh PK. Nucleotide metabolism: a pan-cancer metabolic dependency. Nat Rev Cancer. 2023;23(5):275-94. Epub 2023/03/28. doi: 10.1038/s41568-023-00557-7. PubMed PMID: 36973407; PubMed Central PMCID: PMCPMC10041518.
2. Lesch M, Nyhan WL. A FAMILIAL DISORDER OF URIC ACID METABOLISM AND CENTRAL NERVOUS SYSTEM FUNCTION. Am J Med. 1964;36:561-70. Epub 1964/04/01. doi: 10.1016/0002-9343(64)90104-4. PubMed PMID: 14142409.
3. Giblett ER, Ammann AJ, Wara DW, Sandman R, Diamond LK. Nucleoside-phosphorylase deficiency in a child with severely defective T-cell immunity and normal B-cell immunity. Lancet. 1975;1(7914):1010-3. Epub 1975/05/03. doi: 10.1016/s0140-6736(75)91950-9. PubMed PMID: 48676.
4. Duran M, Beemer FA, van de Heiden C, Korteland J, de Bree PK, Brink M, et al. Combined deficiency of xanthine oxidase and sulphite oxidase: a defect of molybdenum metabolism or transport? J Inherit Metab Dis. 1978;1(4):175-8. Epub 1978/01/01. doi: 10.1007/bf01805591. PubMed PMID: 117254.

5. Dent CE, Philpot GR. Xanthinuria, an inborn error (or deviation) of metabolism. Lancet. 1954;266(6804):182-5. Epub 1954/01/23. doi: 10.1016/s0140-6736(54)91257-x. PubMed PMID: 13118765.
6. Ball EG. XANTHINE OXIDASE: PURIFICATION AND PROPERTIES. J Biol Chem. 1939;128(1):51-67.
7. Sebesta I. Genetic disorders resulting in hyper- or hypouricemia. Adv Chronic Kidney Dis. 2012;19(6):398-403. Epub 2012/10/24. doi: 10.1053/j.ackd.2012.06.002. PubMed PMID: 23089275.
8. Warnhoff K, Ruvkun G. Molybdenum cofactor transfer from bacteria to nematode mediates sulfite detoxification. Nat Chem Biol. 2019;15(5):480-8. Epub 2019/03/27. doi: 10.1038/s41589-019-0249-y. PubMed PMID: 30911177; PubMed Central PMCID: PMCPMC6470025.
9. Schwarz G, Mendel RR, Ribbe MW. Molybdenum cofactors, enzymes and pathways. Nature. 2009;460(7257):839-47. Epub 2009/08/14. doi: 10.1038/nature08302. PubMed PMID: 19675644.
10. Snoozy J, Breen PC, Ruvkun G, Warnhoff K. moc-6/MOCS2A is necessary for molybdenum cofactor synthesis in C. elegans. MicroPubl Biol. 2022;2022. Epub 2022/03/01. doi: 10.17912/micropub.biology.000531. PubMed PMID: 35224462; PubMed Central PMCID: PMCPMC8864482.
11. Warnhoff K, Hercher TW, Mendel RR, Ruvkun G. Protein-bound molybdenum cofactor is bioavailable and rescues molybdenum cofactor-deficient C. elegans. Genes Dev. 2021;35(3-4):212-7. Epub 2021/01/16. doi: 10.1101/gad.345579.120. PubMed PMID: 33446569; PubMed Central PMCID: PMCPMC7849362.
12. Oliphant KD, Fettig RR, Snoozy J, Mendel RR, Warnhoff K. Obtaining the necessary molybdenum cofactor for sulfite oxidase activity in the nematode Caenorhabditis elegans surprisingly involves a dietary source. J Biol Chem. 2023;299(1):102736. Epub 2022/11/25. doi: 10.1016/j.jbc.2022.102736. PubMed PMID: 36423681; PubMed Central PMCID: PMCPMC9793310.
13. Sherman T, Chernova MN, Clark JS, Jiang L, Alper SL, Nehrke K. The abts and sulp families of anion transporters from Caenorhabditis elegans. Am J Physiol Cell Physiol. 2005;289(2):C341-51. Epub 2005/04/09. doi: 10.1152/ajpcell.00071.2005. PubMed PMID: 15814591.
14. Nelson FK, Riddle DL. Functional study of the Caenorhabditis elegans secretory-excretory system using laser microsurgery. J Exp Zool. 1984;231(1):45-56. Epub 1984/07/01. doi: 10.1002/jez.1402310107. PubMed PMID: 6470649.
15. Rohlfing AK, Miteva Y, Moronetti L, He L, Lamitina T. The Caenorhabditis elegans mucin-like protein OSM-8 negatively regulates osmosensitive physiology via the transmembrane protein PTR-23. PLoS Genet. 2011;7(1):e1001267. Epub 2011/01/22. doi: 10.1371/journal.pgen.1001267. PubMed PMID: 21253570; PubMed Central PMCID: PMCPMC3017116.
16. Chalmers RA, Watts RW, Pallis C, Bitensky L, Chayen J. Crystalline deposits in striped muscle in xanthinuria. Nature. 1969;221(5176):170-1. Epub 1969/01/11. doi: 10.1038/221170a0. PubMed PMID: 5782709.
17. Watts RW, Engelman K, Klinenberg JR, Seegmiller JE, Sjoerdsma A. ENZYME DEFECT IN A CASE OF XANTHINURIA. Nature. 1964;201:395-6. Epub 1964/01/25. doi: 10.1038/201395a0. PubMed PMID: 14110004.
18. Ma X, Wang W, Bittner F, Schmidt N, Berkey R, Zhang L, et al. Dual and Opposing Roles of Xanthine Dehydrogenase in Defense-Associated Reactive Oxygen Species Metabolism in Arabidopsis. Plant Cell. 2016;28(5):1108-26. Epub 2016/05/07. doi: 10.1105/tpc.15.00880. PubMed PMID: 27152019; PubMed Central PMCID: PMCPMC4904670.
19. Chi T, Kim MS, Lang S, Bose N, Kahn A, Flechner L, et al. A Drosophila model identifies a critical role for zinc in mineralization for kidney stone disease. PLoS One. 2015;10(5):e0124150.

869 Epub 2015/05/15. doi: 10.1371/journal.pone.0124150. PubMed PMID: 25970330; PubMed
870 Central PMCID: PMCPMC4430225.
871 20. Glassman E, Mitchell HK. Mutants of Drosophila Melanogaster Deficient in Xanthine
872 Dehydrogenase. Genetics. 1959;44(2):153-62. Epub 1959/03/01. doi: 10.1093/genetics/44.2.153.
873 PubMed PMID: 17247815; PubMed Central PMCID: PMCPMC1209939.
874 21. Takagaki N, Ohta A, Ohnishi K, Kawanabe A, Minakuchi Y, Toyoda A, et al. The
875 mechanoreceptor DEG-1 regulates cold tolerance in Caenorhabditis elegans. EMBO Rep.
876 2020;21(3):e48671. Epub 2020/02/06. doi: 10.15252/embr.201948671. PubMed PMID:
877 32009302; PubMed Central PMCID: PMCPMC7054665.
878 22. Brenner S. The genetics of Caenorhabditis elegans. Genetics. 1974;77(1):71-94. Epub
879 1974/05/01. PubMed PMID: 4366476; PubMed Central PMCID: PMCPMC1213120.
880 23. Cho SW, Lee J, Carroll D, Kim JS, Lee J. Heritable gene knockout in Caenorhabditis
881 elegans by direct injection of Cas9-sgRNA ribonucleoproteins. Genetics. 2013;195(3):1177-80.
882 Epub 2013/08/28. doi: 10.1534/genetics.113.155853. PubMed PMID: 23979576; PubMed Central
883 PMCID: PMCPMC3813847.
884 24. Ghanta KS, Mello CC. Melting dsDNA Donor Molecules Greatly Improves Precision
885 Genome Editing in Caenorhabditis elegans. Genetics. 2020;216(3):643-50. Epub 2020/09/24. doi:
886 10.1534/genetics.120.303564. PubMed PMID: 32963112; PubMed Central PMCID:
887 PMCPMC7648581.
888 25. Tecle E, Chhan CB, Franklin L, Underwood RS, Hanna-Rose W, Troemel ER. The purine
889 nucleoside phosphorylase pnp-1 regulates epithelial cell resistance to infection in C. elegans.
890 PLoS Pathog. 2021;17(4):e1009350. Epub 2021/04/21. doi: 10.1371/journal.ppat.1009350.
891 PubMed PMID: 33878133; PubMed Central PMCID: PMCPMC8087013.
892 26. Altschul SF, Gish W, Miller W, Myers EW, Lipman DJ. Basic local alignment search tool. J
893 Mol Biol. 1990;215(3):403-10. Epub 1990/10/05. doi: 10.1016/s0022-2836(05)80360-2. PubMed
894 PMID: 2231712.
895 27. Buechner M. Tubes and the single C. elegans excretory cell. Trends Cell Biol.
896 2002;12(10):479-84. Epub 2002/11/21. doi: 10.1016/s0962-8924(02)02364-4. PubMed PMID:
897 12441252.
898 28. Suzuki N, Buechner M, Nishiwaki K, Hall DH, Nakanishi H, Takai Y, et al. A putative GDP-
899 GTP exchange factor is required for development of the excretory cell in Caenorhabditis elegans.
900 EMBO Rep. 2001;2(6):530-5. Epub 2001/06/21. doi: 10.1093/embo-reports/kve110. PubMed
901 PMID: 11415987; PubMed Central PMCID: PMCPMC1083904.
902 29. Branicky R, Hekimi S. What keeps C. elegans regular: the genetics of defecation. Trends
903 Genet. 2006;22(10):571-9. Epub 2006/08/17. doi: 10.1016/j.tig.2006.08.006. PubMed PMID:
904 16911844.
905 30. Thomas JH. Genetic analysis of defecation in Caenorhabditis elegans. Genetics.
906 1990;124(4):855-72. Epub 1990/04/01. doi: 10.1093/genetics/124.4.855. PubMed PMID:
907 2323555; PubMed Central PMCID: PMCPMC1203977.
908 31. Warnhoff K, Bhattacharya S, Snoozy J, Breen PC, Ruvkun G. Hypoxia-inducible factor
909 induces cysteine dioxygenase and promotes cysteine homeostasis in Caenorhabditis elegans.
910 Elife. 2024;12. Epub 2024/02/13. doi: 10.7554/eLife.89173. PubMed PMID: 38349720.
911 32. Stipanuk MH, Ueki I. Dealing with methionine/homocysteine sulfur: cysteine metabolism to
912 taurine and inorganic sulfur. J Inherit Metab Dis. 2011;34(1):17-32. Epub 2010/02/18. doi:
913 10.1007/s10545-009-9006-9. PubMed PMID: 20162368; PubMed Central PMCID:
914 PMCPMC2901774.
915 33. Dissanayake LV, Zietara A, Levchenko V, Spires DR, Burgos Angulo M, El-Meanawy A, et
916 al. Lack of xanthine dehydrogenase leads to a remarkable renal decline in a novel hypouricemic
917 rat model. iScience. 2022;25(9):104887. Epub 2022/08/31. doi: 10.1016/j.isci.2022.104887.
918 PubMed PMID: 36039296; PubMed Central PMCID: PMCPMC9418856.

919 34. Rohlfing AK, Miteva Y, Hannenhalli S, Lamitina T. Genetic and physiological activation of
920 osmosensitive gene expression mimics transcriptional signatures of pathogen infection in C.
921 elegans. PLoS One. 2010;5(2):e9010. Epub 2010/02/04. doi: 10.1371/journal.pone.0009010.
922 PubMed PMID: 20126308; PubMed Central PMCID: PMCPMC2814864.
923 35. Lamitina T, Huang CG, Strange K. Genome-wide RNAi screening identifies protein
924 damage as a regulator of osmoprotective gene expression. Proc Natl Acad Sci U S A.
925 2006;103(32):12173-8. Epub 2006/08/02. doi: 10.1073/pnas.0602987103. PubMed PMID:
926 16880390; PubMed Central PMCID: PMCPMC1567714.
927 36. Lamitina ST, Morrison R, Moeckel GW, Strange K. Adaptation of the nematode
928 Caenorhabditis elegans to extreme osmotic stress. Am J Physiol Cell Physiol. 2004;286(4):C785-
929 91. Epub 2003/12/03. doi: 10.1152/ajpcell.00381.2003. PubMed PMID: 14644776.
930 37. Kage-Nakadai E, Uehara T, Mitani S. H+/myo-inositol transporter genes, hmit-1.1 and
931 hmit-1.2, have roles in the osmoprotective response in Caenorhabditis elegans. Biochem Biophys
932 Res Commun. 2011;410(3):471-7. Epub 2011/06/18. doi: 10.1016/j.bbrc.2011.06.001. PubMed
933 PMID: 21679696.
934 38. Lee SD, Choi SY, Lim SW, Lamitina ST, Ho SN, Go WY, et al. TonEBP stimulates multiple
935 cellular pathways for adaptation to hypertonic stress: organic osmolyte-dependent and -
936 independent pathways. Am J Physiol Renal Physiol. 2011;300(3):F707-15. Epub 2011/01/07. doi:
937 10.1152/ajprenal.00227.2010. PubMed PMID: 21209002; PubMed Central PMCID:
938 PMCPMC3064130.
939 39. Pais VM, Jr., Lowe G, Lallas CD, Preminger GM, Assimos DG. Xanthine urolithiasis.
940 Urology. 2006;67(5):1084.e9-11. Epub 2006/05/16. doi: 10.1016/j.urology.2005.10.057. PubMed
941 PMID: 16698380.
942 40. Yanagi KS, Jochim B, Kunjo SO, Breen P, Ruvkun G, Lehrbach N. Mutations in nucleotide
943 metabolism genes bypass proteasome defects in png-1/NGLY1-deficient Caenorhabditis elegans.
944 PLoS Biol. 2024;22(7):e3002720. Epub 2024/07/11. doi: 10.1371/journal.pbio.3002720. PubMed
945 PMID: 38991033; PubMed Central PMCID: PMCPMC11265709.
946 41. Ast T, Meisel JD, Patra S, Wang H, Grange RMH, Kim SH, et al. Hypoxia Rescues
947 Frataxin Loss by Restoring Iron Sulfur Cluster Biogenesis. Cell. 2019;177(6):1507-21.e16. Epub
948 2019/04/30. doi: 10.1016/j.cell.2019.03.045. PubMed PMID: 31031004; PubMed Central PMCID:
949 PMCPMC6911770.
950 42. Bantia S, Parker C, Upshaw R, Cunningham A, Kotian P, Kilpatrick JM, et al. Potent orally
951 bioavailable purine nucleoside phosphorylase inhibitor BCX-4208 induces apoptosis in B- and T-
952 lymphocytes--a novel treatment approach for autoimmune diseases, organ transplantation and
953 hematologic malignancies. Int Immunopharmacol. 2010;10(7):784-90. Epub 2010/04/20. doi:
954 10.1016/j.intimp.2010.04.009. PubMed PMID: 20399911.
955 43. Kamath VP, Juarez-Brambila JJ, Morris PE, Jr. Synthesis of labeled BCX-4208, a potent
956 inhibitor of purine nucleoside phosphorylase. Drug Test Anal. 2009;1(3):125-7. Epub 2010/04/01.
957 doi: 10.1002/dta.24. PubMed PMID: 20355185.
958 44. Adrogué HJ, Madias NE. Hypernatremia. N Engl J Med. 2000;342(20):1493-9. Epub
959 2000/05/18. doi: 10.1056/nejm200005183422006. PubMed PMID: 10816188.
960 45. Prince CL, Scardino PL, Wolan CT. The effect of temperature, humidity and dehydration on
961 the formation of renal calculi. J Urol. 1956;75(2):209-15. Epub 1956/02/01. doi: 10.1016/s0022-
962 5347(17)66798-3. PubMed PMID: 13296117.
963 46. Mudd SH, Irreverre F, Laster L. Sulfite oxidase deficiency in man: demonstration of the
964 enzymatic defect. Science. 1967;156(3782):1599-602. Epub 1967/06/23. doi:
965 10.1126/science.156.3782.1599. PubMed PMID: 6025118.
966 47. Dominy JE, Jr., Hirschberger LL, Coloso RM, Stipanuk MH. In vivo regulation of cysteine
967 dioxygenase via the ubiquitin-26S proteasome system. Adv Exp Med Biol. 2006;583:37-47. Epub
968 2006/12/13. doi: 10.1007/978-0-387-33504-9_4. PubMed PMID: 17153587.

969 48. Dominy JE, Jr., Hirschberger LL, Coloso RM, Stipanuk MH. Regulation of cysteine
970 dioxygenase degradation is mediated by intracellular cysteine levels and the ubiquitin-26 S
971 proteasome system in the living rat. Biochem J. 2006;394(Pt 1):267-73. Epub 2005/11/03. doi:
972 10.1042/bj20051510. PubMed PMID: 16262602; PubMed Central PMCID: PMCPMC1386025.
973 49. Stipanuk MH, Hirschberger LL, Londono MP, Cresenzi CL, Yu AF. The ubiquitin-
974 proteasome system is responsible for cysteine-responsive regulation of cysteine dioxygenase
975 concentration in liver. Am J Physiol Endocrinol Metab. 2004;286(3):E439-48. Epub 2003/12/03.
976 doi: 10.1152/ajpendo.00336.2003. PubMed PMID: 14644768.
977 50. Lee JI, Londono M, Hirschberger LL, Stipanuk MH. Regulation of cysteine dioxygenase
978 and gamma-glutamylcysteine synthetase is associated with hepatic cysteine level. J Nutr
979 Biochem. 2004;15(2):112-22. Epub 2004/02/20. doi: 10.1016/j.jnutbio.2003.10.005. PubMed
980 PMID: 14972351.
981 51. Kwon YH, Stipanuk MH. Cysteine regulates expression of cysteine dioxygenase and
982 gamma-glutamylcysteine synthetase in cultured rat hepatocytes. Am J Physiol Endocrinol Metab.
983 2001;280(5):E804-15. Epub 2001/04/05. doi: 10.1152/ajpendo.2001.280.5.E804. PubMed PMID:
984 11287364.
985 52. Hill AJ, Basourakos SP, Lewicki P, Wu X, Arenas-Gallo C, Chuang D, et al. Incidence of
986 Kidney Stones in the United States: The Continuous National Health and Nutrition Examination
987 Survey. J Urol. 2022;207(4):851-6. Epub 2021/12/03. doi: 10.1097/ju.0000000000002331.
988 PubMed PMID: 34854755.
989 53. Jiang Z, Asplin JR, Evan AP, Rajendran VM, Velazquez H, Nottoli TP, et al. Calcium
990 oxalate urolithiasis in mice lacking anion transporter Slc26a6. Nat Genet. 2006;38(4):474-8. Epub
991 2006/03/15. doi: 10.1038/ng1762. PubMed PMID: 16532010.
992 54. Cornière N, Thomson RB, Thauvin S, Villoutreix BO, Karp S, Dynia DW, et al. Dominant
993 negative mutation in oxalate transporter SLC26A6 associated with enteric hyperoxaluria and
994 nephrolithiasis. J Med Genet. 2022;59(11):1035-43. Epub 2022/02/05. doi: 10.1136/jmedgenet-
995 2021-108256. PubMed PMID: 35115415; PubMed Central PMCID: PMCPMC9346097.
996 55. Gee HY, Jun I, Braun DA, Lawson JA, Halbritter J, Shril S, et al. Mutations in SLC26A1
997 Cause Nephrolithiasis. Am J Hum Genet. 2016;98(6):1228-34. Epub 2016/05/24. doi:
998 10.1016/j.ajhg.2016.03.026. PubMed PMID: 27210743; PubMed Central PMCID:
999 PMCPMC4908148.
1000 56. Hirata T, Cabrero P, Berkholz DS, Bondeson DP, Ritman EL, Thompson JR, et al. In vivo
1001 Drosophilia genetic model for calcium oxalate nephrolithiasis. Am J Physiol Renal Physiol.
1002 2012;303(11):F1555-62. Epub 2012/09/21. doi: 10.1152/ajprenal.00074.2012. PubMed PMID:
1003 22993075; PubMed Central PMCID: PMCPMC3532482.
1004 57. Baba T, Ara T, Hasegawa M, Takai Y, Okumura Y, Baba M, et al. Construction of
1005 Escherichia coli K-12 in-frame, single-gene knockout mutants: the Keio collection. Mol Syst Biol.
1006 2006;2:2006.0008. Epub 2006/06/02. doi: 10.1038/msb4100050. PubMed PMID: 16738554;
1007 PubMed Central PMCID: PMCPMC1681482.
1008 58. Mattingly BC, Buechner M. The FGD homologue EXC-5 regulates apical trafficking in C.
1009 elegans tubules. Dev Biol. 2011;359(1):59-72. Epub 2011/09/06. doi:
1010 10.1016/j.ydbio.2011.08.011. PubMed PMID: 21889936; PubMed Central PMCID:
1011 PMCPMC3212395.
1012 59. Lehrbach NJ, Ji F, Sadreyev R. Next-Generation Sequencing for Identification of EMS-
1013 Induced Mutations in Caenorhabditis elegans. Curr Protoc Mol Biol. 2017;117:7.29.1-7..12. Epub
1014 2017/01/07. doi: 10.1002/cpmb.27. PubMed PMID: 28060408; PubMed Central PMCID:
1015 PMCPMC5303615.
1016 60. Community G. The Galaxy platform for accessible, reproducible and collaborative
1017 biomedical analyses: 2022 update. Nucleic Acids Res. 2022;50(W1):W345-51. Epub 2022/04/22.
1018 doi: 10.1093/nar/gkac247. PubMed PMID: 35446428; PubMed Central PMCID:
1019 PMCPMC9252830.

1020 61. Bolger AM, Lohse M, Usadel B. Trimmomatic: a flexible trimmer for Illumina sequence
1021 data. Bioinformatics. 2014;30(15):2114-20. Epub 2014/04/04. doi: 10.1093/bioinformatics/btu170.
1022 PubMed PMID: 24695404; PubMed Central PMCID: PMCPMC4103590.
1023 62. Li H, Durbin R. Fast and accurate long-read alignment with Burrows-Wheeler transform.
1024 Bioinformatics. 2010;26(5):589-95. Epub 2010/01/19. doi: 10.1093/bioinformatics/btp698.
1025 PubMed PMID: 20080505; PubMed Central PMCID: PMCPMC2828108.
1026 63. Wilm A, Aw PP, Bertrand D, Yeo GH, Ong SH, Wong CH, et al. LoFreq: a sequence-quality
1027 aware, ultra-sensitive variant caller for uncovering cell-population heterogeneity from high-
1028 throughput sequencing datasets. Nucleic Acids Res. 2012;40(22):11189-201. Epub 2012/10/16.
1029 doi: 10.1093/nar/gks918. PubMed PMID: 23066108; PubMed Central PMCID:
1030 PMCPMC3526318.
1031 64. Cingolani P, Patel VM, Coon M, Nguyen T, Land SJ, Ruden DM, et al. Using Drosophila
1032 melanogaster as a Model for Genotoxic Chemical Mutational Studies with a New Program,
1033 SnpSift. Front Genet. 2012;3:35. Epub 2012/03/22. doi: 10.3389/fgene.2012.00035. PubMed
1034 PMID: 22435069; PubMed Central PMCID: PMCPMC3304048.
1035 65. Cingolani P, Platts A, Wang le L, Coon M, Nguyen T, Wang L, et al. A program for
1036 annotating and predicting the effects of single nucleotide polymorphisms, SnpEff: SNPs in the
1037 genome of Drosophila melanogaster strain w1118; iso-2; iso-3. Fly (Austin). 2012;6(2):80-92.
1038 Epub 2012/06/26. doi: 10.4161/fly.19695. PubMed PMID: 22728672; PubMed Central PMCID:
1039 PMCPMC3679285.
1040 66. Mello CC, Kramer JM, Stinchcomb D, Ambros V. Efficient gene transfer in C.elegans:
1041 extrachromosomal maintenance and integration of transforming sequences. Embo j.
1042 1991;10(12):3959-70. Epub 1991/12/01. doi: 10.1002/j.1460-2075.1991.tb04966.x. PubMed
1043 PMID: 1935914; PubMed Central PMCID: PMCPMC453137.
1044 67. Stiernagle T. Maintenance of C. elegans. WormBook. 2006:1-11. Epub 2007/12/01. doi:
1045 10.1895/wormbook.1.101.1. PubMed PMID: 18050451; PubMed Central PMCID:
1046 PMCPMC4781397.
1047 68. Schmittgen TD, Livak KJ. Analyzing real-time PCR data by the comparative C(T) method.
1048 Nat Protoc. 2008;3(6):1101-8. Epub 2008/06/13. doi: 10.1038/nprot.2008.73. PubMed PMID:
1049 18546601.
1050
1051
1052
1053
1054
1055
1056
1057
1058
1059
1060
1061
1062
1063
1064

1065 **Supporting Information:**

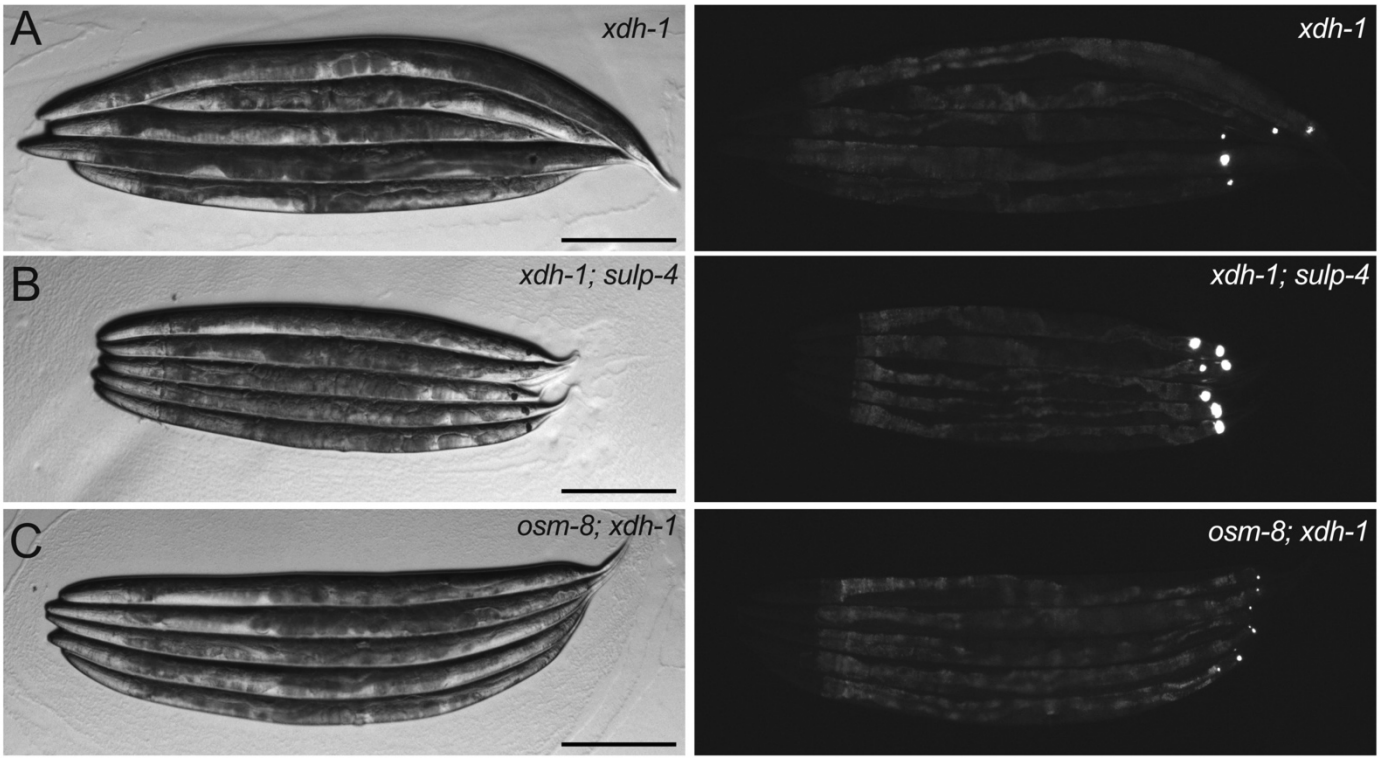

1066

1067 **Figure S1:** Loss of *sulp-4* enhanced the expressivity of the xanthine stone phenotype displayed by *xdh-1*
1068 mutant animals.
1069 Brightfield (left) and fluorescent (right) images of A) *xdh-1(ok3234),* B) *xdh-1(ok3234); sulp-4(rae319),* or
1070 C) *osm-8(n1518); xdh-1(ok3234)* mutant adult *C. elegans* cultured on wild-type *E. coli.* Scale bar is
1071 250μm. Note, *xdh-1(ok3234)* animals displayed are older than their *xdh-1(ok3234); sulp-4(rae319)* or *osm-*
1072 *8(n1518); xdh-1(ok3234)* counterparts which were imaged as day 2 adults. This was necessary to allow us
1073 to identify sufficient *xdh-1* single mutant animals displaying a xanthine stone.

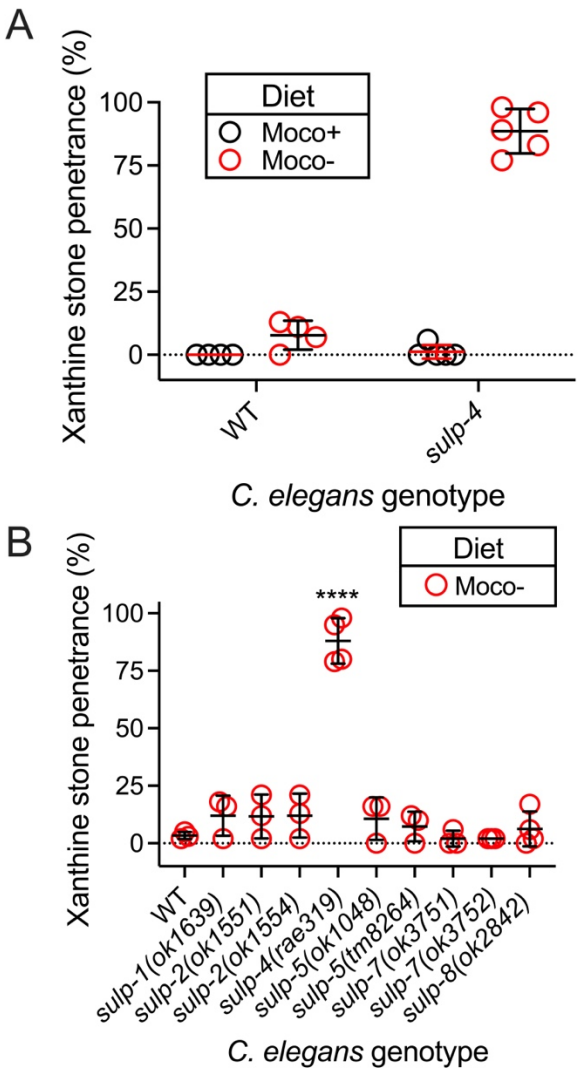

Figure S2: Inactivating mutations in *sulp* genes other than *sulp-4* did not enhance xanthine stone formation during dietary Moco deficiency.

A) Wild-type and *sulp-4(rae319) C. elegans* were cultured on wild-type (black, Moco+) or *ΔmoaA* mutant (red, Moco-) *E. coli* and assessed for the formation of xanthine stones. Note, data points for the wild-type animals cultured on Moco+ and Moco- *E. coli* are derived from the same experiment that is displayed in **Fig. 1B** However, in this analysis the animals were scored until day 4 of adulthood. B) Wild type and viable *sulp* mutant *C. elegans* were cultured on *ΔmoaA* mutant (red, Moco-) *E. coli* and assessed for the formation of xanthine stones. Data points represent biological replicates. ****, $p<0.0001$, ordinary one-way ANOVA. If not indicated, data were not statistically different when compared to the wild type. Complete information regarding individuals scored per biological replicate are found in **Table S2**.

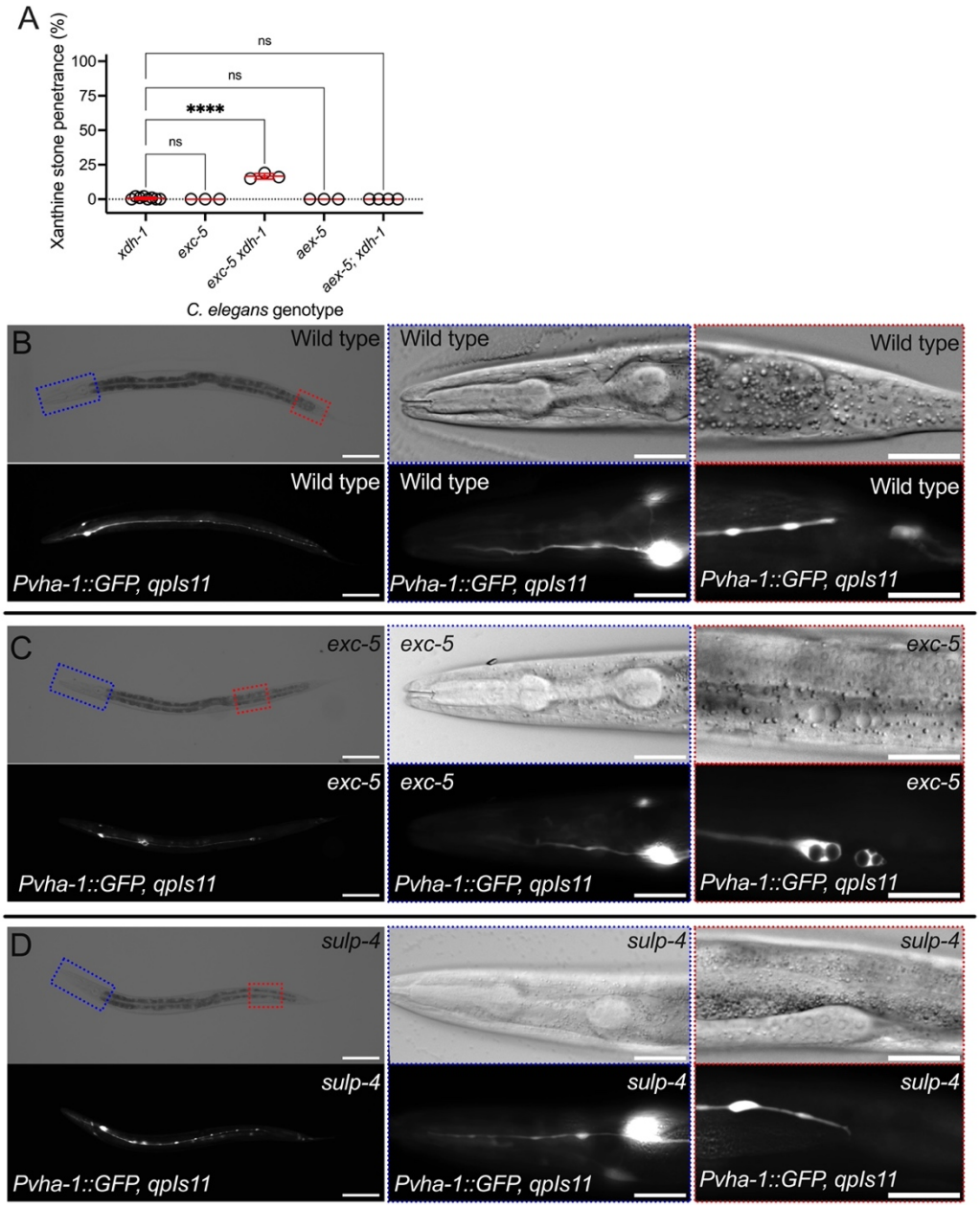

Figure S3: Loss of *exc-5* modestly enhanced the formation of xanthine stones in an *xdh-1* mutant background.

A) *xdh-1(ok3234), exc-5(rh232), exc-5(rh232) xdh-1(ok3234), aex-5(sa23),* and *aex-5(sa23); xdh-1(ok3234)* mutant *C. elegans* were assessed for xanthine stone formation when cultured on wild-type *E. coli*. Individual data points represent biological replicates. Mean and standard deviation are displayed. ****, $p<0.0001$, ns, $p>0.05$, ordinary one-way ANOVA. Complete information regarding sample size and individuals scored per biological replicate are found in **Table S2**. B-D) Differential interference contrast (top) and fluorescence imaging (bottom) are displayed for B) wild-type, C) *exc-5(rh232),* or D) *sulp-4(rae319) C. elegans* expressing the *qpIs11* (*Pvha-1::GFP)* transgene, which marks the excretory cell. For images of whole animals (left panels), the blue (anterior) and red (posterior) boxes identify the regions displayed in the panels on the right. For images of whole animals (left panels), scale bar is 100μm. For images of anterior (blue box) and posterior (red box) excretory cell tubule extension, scale bar is 25μm.

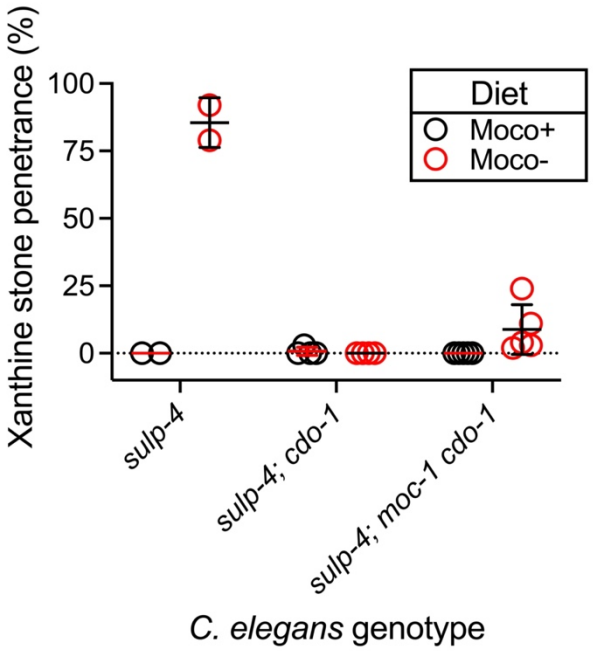

Figure S4: *cdo-1* was necessary for the enhanced formation of xanthine stones caused by *sulp-4* inactivation during dietary Moco deficiency.

sulp-4(rae319), sulp-4(rae319); cdo-1(mg622), and *sulp-4(rae319); moc-1(ok366) cdo-1(mg622)* mutant *C. elegans* were cultured on wild-type (black, Moco+) or *ΔmoaA* mutant (red, Moco-) *E. coli* and assessed for the formation of xanthine stones over the first 3 days of adulthood. Mean and standard deviation are displayed. Complete information regarding sample size and individuals scored per biological replicate are found in **Table S2**.

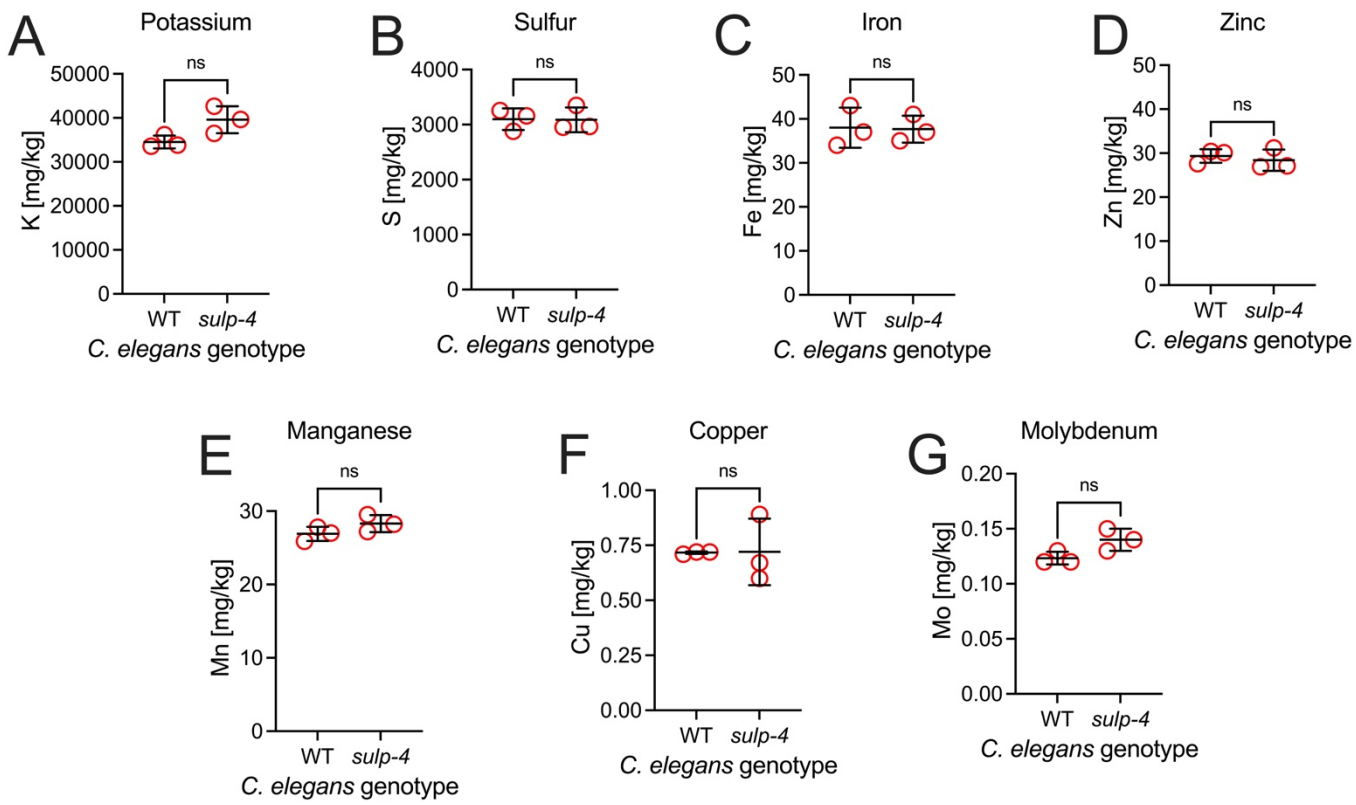

Figure S5: Elemental analyses of wild-type and *sulp-4* mutant *C. elegans.* ICP-MS analysis was performed on extracts from large cultures of young adult wild-type and *sulp-4(rae319)* mutant *C. elegans* to determine the concentrations of A) potassium, B) sulfur, C) iron, D) zinc, E) manganese, F) copper, and G) molybdenum. Individual data points represent biological replicates. Mean and standard deviation are displayed. ns, p>0.05, t test.

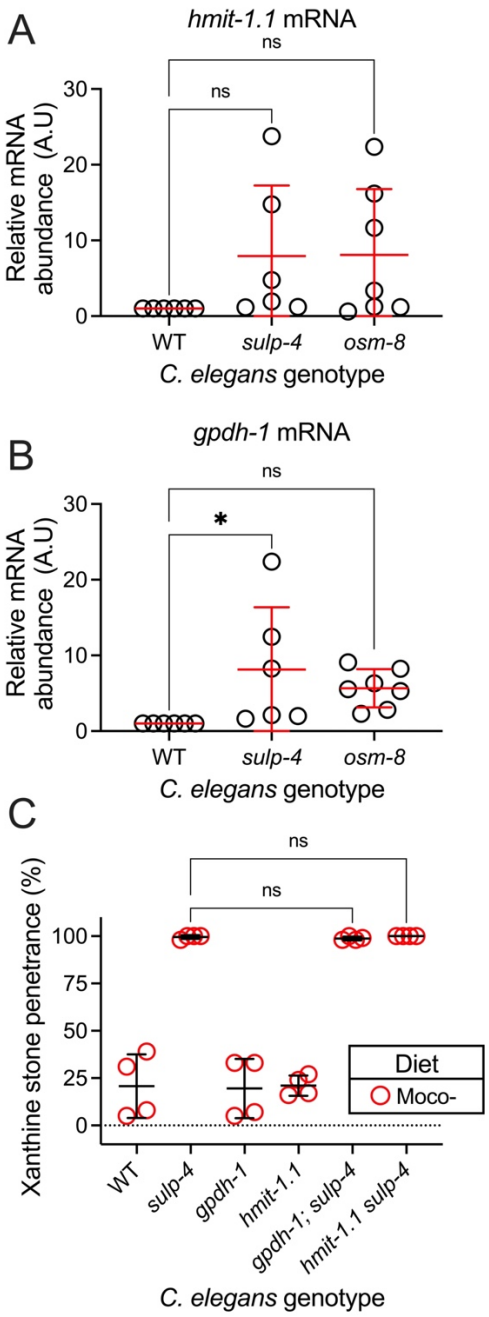

Figure S6: *hmit-1.1* and *gpdh-1* were not necessary for the enhanced formation of xanthine stones caused by *sulp-4* inactivation during dietary Moco deficiency.

Relative mRNA expression of A) *hmit-1.1* and B) *gpdh-1* are displayed for total RNA isolated from wild-type, *sulp-4(rae319)*, and *osm-8(n1518)* young adult *C. elegans.* Relative mRNA abundance was determined via the delta-delta C_T method. All transcripts are normalized to *act-1.* Relative mRNA abundance for each transcript was set to one in the wild type. *, $p<0.05$, ns, $p>0.05$, ordinary one-way ANOVA. C) Wild type and mutant *C. elegans* were cultured on *ΔmoaA* mutant (red, Moco-) *E. coli* and assessed for the formation of xanthine stones. Individual data points represent biological replicates. Mean and standard deviation are displayed. ns, $p>0.05$, ordinary one-way ANOVA. Complete information regarding sample size and individuals scored per biological replicate are found in **Table S2**.

Strain	Allele	Chromosome	Chromosome position	Gene affected	Reference base	Mutant base	Allele status	Variant impact
USD962	*rae299*	V	11876913	*sulp-4*	C	T	Homozygous	Pro325Leu
USD971	*rae302*	V	11877161	*sulp-4*	G	A	Homozygous	Splice donor variant
USD990	*rae319*	V	11875799	*sulp-4*	G	A	Homozygous	Gly116Glu
USD1013	*rae320*	V	11875799	*sulp-4*	G	A	Homozygous	Gly116Glu
USD1019	*rae326*	V	11878726	*sulp-4*	G	A	Homozygous	Splice acceptor variant

Table S1: EMS-induced lesions in *sulp-4* that promoted the formation of xanthine stones in *xdh-1(ok3234)*-mutant *C. elegans.*

Table S2: Raw data and information regarding sample sizes and biological replicates. Too large to be embedded in manuscript.